Titel:
Title: COMPERE Final Report -- DLR Contract Number 50 JR 0012

Dokumenten Typ:
Document Type: Technical Note

Konfigurations-Nr.:
Configuration Item No.: -

Referenz- Nr.:
Reference No.: DLR FKZ Number: 50 JR 0012

Klassifikations-Nr.:
Classification No.: -

Lieferbedingungs-Nr.:
DRL/DRD No.:

Freigabe Nr.:
Release No.: -

Gruppierung (Dok.):
Group (Doc.-related): -

**Gruppierung (Version):**
Group (Version-related): -

Thema:
Subject:

Kurzbeschreibung:
Abstract:

The present report describes the activities which were carried out in the frame of the COMPERE project. Goal of the COMPERE project is to prepare the next generation of cryogenic upper stage developments. Main focus is to assess and develop the capabilities of numerical software codes such as FLOW-3D which are required for future analyses. A number of benchmark experiments were therefore generated which allow a crosscheck with the computer codes. The results show that in major parts the computer codes are well able to describe the physical phenomena. The combined analyses of mechanical and thermal problems, e.g. the assessment of boiling phenomena in upper stage tanks, however require further investigation.

Autor:
Prepared by: M. Winter
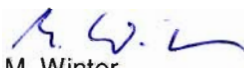
Org. Einh.:
Organ. Unit: TE 51

Unternehmen: Astrium GmbH
Company: Astrium GmbH

Geprüft:
Agreed by: Dr. P. Behruzi

Org. Einh.:
Organ. Unit: TE 51

Unternehmen: Astrium GmbH
Company:

Genehmigt:
Approved by: Dr. Rittweger

Org. Einh.:
Organ. Unit: TE 51

Unternehmen:
Company: Astrium GmbH

Genehmigt:
Approved by:

Org. Einh.:
Organ. Unit:

Unternehmen:
Company:

Daten/Dokument-Änderungsnachweis/Data/Document Change Record (DCR)

Ausgabe Issue	Datum Date	Betroffener Abschnitt/Paragraph/Seite Affected Section/Paragraph/Page	Änderungsgrund/Kurze Änderungsbeschreibung Reason for Change/Brief Description of Change
1	15.06.07	All	Initial Issue

Inhaltsverzeichnis/Table of Contents (ToC)

1. Introduction

The present report describes the activities which were carried out in the frame of the COMPERE project. The COMPERE group presently includes the following members (alphabetic order):

- Air Liquide
- CNES
- Cryospace
- DLR
- EADS ASTRIUM Space Transportation (Bremen, Germany and Les Mureaux, France)
- IMFT (Institut Mechanique des Fluides de Toulouse)
- LEGI
- ONERA
- University of Erlangen
- ZARM Bremen

Goal of the COMPERE project is to prepare the next generation of cryogenic upper stage developments. Since new stage developments tend towards coasting phases of variable durations, which can not be realized with the presently used Ariane 5 upper stage ESC-A, a number of new flight phases have to be assessed. These include:

- the propulsive phase,
- the engine shut-down phase,
- the ballistic phase,
- and the preparatory phase for engine restart (tank depressurization, engine chilldown, …).

To assess these flight phases a number of physical phenomena have to be well understood. A number of phenomena are mentioned below:

- Sloshing, non linear effects, initiation of break-up
- Amplification of sloshing including geometric effects
- Formation of droplets
- Droplet and bubble formation by break-up
- Vaporization of droplets due to thermal effects or/and concentration
- Heat and mass transfer at interface and walls
- Thermal stratification in draining phase
- Heat and mass transfer at interface and walls
- Vaporization of droplets due to thermal effects or/and concentration

The project goals with respect to the most important future tasks have been defined in common by all COMPERE members. It is therefore common practice in the group that all performed work packages are discussed within the group in order to make sure that the goals of all partners are in line with the required future developments.

The numerical modelization of the above mentioned physical phenomena impose many new features for the used CFD tools (for Astrium mainly the FLOW-3D software). A clear understanding of the code capabilities exists however only partly. Information concerning accuracy has been very limited before the COMPERE project. It is therefore the major goal of the COMPERE project to close this gap and to develop the used computer codes for the coming upper stage and satellite developments. A number of benchmark experiments were therefore generated which allow a crosscheck with the computer codes.

In the following the objectives of the COMPERE project will be shortly described. The scientific status at the beginning of the project will be highlighted. Furthermore the different tasks performed within the project will be given. Finally a short assessment of the achieved results and an outlook concerning the required next steps will be given.

2. References

[RD 1]   Rapport d'expertise COMPERE RT 75/6116 DEFA/Y, Parts 1 and 2, ONERA, 1999

[RD 2]   Behruzi, P., Netter, G., "Flüssigkeitshandhabung in Raketenoberstufen und Transfer Vehikeln unter Berücksichtigung ballistischer Phasen (0g)", Deutscher Luft- und Raumfahrt Kongress, Stuttgart, 2002

[RD 3]   Jaekle Jr., D. E., "Propellant Management Device Conceptual Design and Analysis: Traps and Troughs", AIAA-95-2531, 1995

[RD 4]   Behruzi, K. P., Netter, G., Müller, R., "Propellant Settling of Ariane 5 EPSV Upper Stage", 4th Int. Conf. on Launcher Techn., Liège, 3-6 Dec. 2002

[RD 5]   Colin, C., "Analysis of the wall heat transfers in nucleate boiling in micro gravity: Application to the propellant tanks of Ariane 5", Institut de Mécanique des Fluides de Toulouse, Compere Program, 2001

[RD 6]   Chato, D. J., "Technologies for Refueling Spacecraft On-Orbit", AIAA-2000-5107, Nov. 2000

[RD 7]   Blatt, M. H., Walter, M. D., "Centaur Propellant Acquisition System Study", NASA CR-134811, 1975

[RD 8]   P. Behruzi, G. Netter, "Concept Analysis of PMD Designs for Future Upper Stages", IAF Congress, Bremen, 2003

[RD 9]   D. Haake, Studienarbeit at EADS-ST, "Dreidimensionales Flüssigkeitsschwappen in einem zylindrischen Behälter bei lateraler Anregung und großen Bond-Zahlen, Oct. 2002

[RD 10] Vigletti, B., Modelling of bubbles and drop formation and their motion for different acceleration levels, 2005, TE51-RIBRE-TN-0050

[RD 11] J. Straub, "Boiling Heat Transfer and Bubble Dynamics in Microgravity", Advances in heat Transfer, Vol, 35, 2001

[RD 12] J. Betz, J, Straub, "Numerical and experimental study of the heat transfer and fluid flow by thermo-capillary convection around gas bubbles", Journal of Heat and Mass Transfer, 37, pp. 215-227, 2001

3. List of Acronyms

ATV	Automated Transfer Vehicle
CFD	Computational Fluid Dynamic
COMPERE	COMPortement des Ergols dans les Reservoirs
CNES	Centre national d'études spatiales
DLR	Deutsches Zentrum für Luft- und Raumfahrt
EPS	Etage à Propergol Stockable
ESA	European Space Agency
ESC-A	Etage Supérieur Cryogénique version A
ESC-B	Etage Supérieur Cryogénique version B
ISS	International Space Station
LEGI	Laboratoire des Ecoulements Géophysiques et Industriels
LH2	Liquid Hydrogen
LN2	Liquid Nitrogen
LOX	Liquid Oxygen
IMFT	Institut Mechanique des Fluides de Toulouse)
MMH	Monomethyl Hydrazine
NTO	Nitrogen tetroxide
ONERA	Office National d'Études et de Recherches Aérospatiales
OST	Oberflächenspannungstank
PMD	Propellant Management Device
PRR	Propellant
SCA	System de Control des Attitude
S/W	Software
UDF	User Defined Function
ZARM	Zentrum für angewandte Raumfahrttechnologie und Mikrogravitation

4. Short Documentation

4.1 Task Description

The main objective of the COMPERE program is to improve the scientific knowledge concerning all the phenomena occurring in a tank of a launcher during its flight. COMPERE focuses on the phenomena in relation to the ballistic phase of the flight including the transition between boosted and ballistic periods. The second goal of the COMPERE program is to provide models or correlations which allow taking into account these phenomena in the CFD or engineering tools used by industrials in charge of space tank developments.

For space applications the FLOW-3D software is the software commonly used at EADS Astrium in order to modelise the behaviour of propellants in upper stage and surface tension tanks. Main goal is thus to improve the functional layout process. As an example Fig. 1 shows a satellite configuration including a propellant management device and a configuration of the Ariane 5 ESC-B upper stage which is an option for the next generation of upper stages.
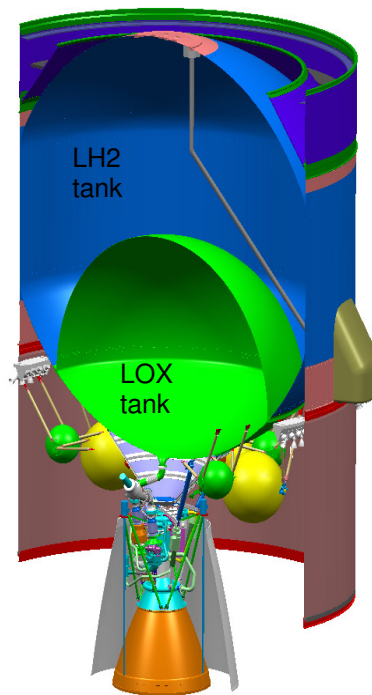

Fig. 1: Ariane 5 upper stage ESC-B (right)

Both, satellite and upper stage require the capability to handle longer coasting phases, around 10 to 15 years for the satellite and in the order of 6 hours for the cryogenic upper stage.

The technical specification of the COMPERE program is based on the present upper stages which include the EPS (Etage à Propergol Stockable), the ESC-A (Etage Supérieur Cryogénique version A) and the future version of the Ariane 5 upper stage. For each stage some parts of the flight are in relation with the phenomena covered by the COMPERE perimeter. For future development of cryogenic upper stages this new stage will include specific features necessary to fulfil the new specifications which include long ballistic phases (some hours) and re-ignitions of the main engine. This is the core of the COMPERE work. Applications linked to the two other upper stages EPS and ESC-A as well as satellite tank developments are also of interests in the frame of COMPERE.

4.2 Requirements by which the project was performed

Frameworks of the COMPERE work are technical requirements which have been defined in the frame of the COMPERE group. The main technical specifications have been summarized in [RD 1] which is the basis for the work performed within the project. Specifications are given for a storable upper stage (i.e. EPS) and a cryogenic upper stage (i.e. ESC type).

4.3 Planning and Schedule of the Project

The planning of the project has to go in line with the work of the other COMPERE members in order to gain the best benefit from the combined work. It is therefore common practice to discuss schedules and future planning with the members and agree on planning as well as schedule on a yearly basis. All tasks have been proposed by the Scientific Committee and were agreed by the Steering Committee.

4.4 Scientific and technical status at the beginning of the Project

4.4.1 Layout and development of surface tension tanks for satellites and upper stages

The layout of surface tension tanks for satellites and upper stages is the main basis for the work carried out in the frame of the COMPERE project. Satellite tanks require propellant storage and expulsion over a long period with numerous engine restarts. Generally the flow rates are, in contrast to upper stages, very low.

The purpose of propellant tanks is to store propellants and to deliver it to the stage's engine whenever needed. A gas / vapour free propellant expulsion from the tank has to be assured since vapour entering the pumps may produce cavitation, poor engine operation and possible feed system failure. In case of upper stages this has been accomplished in the frame of Ariane 4 and Ariane 5 for single boost missions. Multi-boost missions lead to further difficulties since low gravity coast, vehicle drag and disturbing accelerations may position propellant away from the tank outlet. The location of the propellant in the tank is under these circumstances difficult to predict due to the variation of the g vector and an unstable propellant location. Thus means must be provided to position liquid in the feed lines and over the tank outlet.

Two different techniques may be used to insure gas free expulsion:

1. To settle sufficient propellant stable at the tank outlet using additional thrusters prior to the restart of the main engine. This method is planned for Ariane 5 EPS-V missions in combination with the Automatic Transfer Vehicle (ATV). Goal of the ATV mission is to supply the space station ISS and to re-boost the ISS to a higher orbit with the ATV. Settling will be performed using small hydrazine thrusters (called SCA thrusters in case of EPS-V). SCA is used for a pre-acceleration of the EPS-V. This method imposes mission constraints in waiting for propellant to be settled and weight penalties (propellant for pre-acceleration) which are a function of the number of engine burns.

2.
   To accommodate sufficient propellant in a kind of reservoir in order to start the main engine. The propellant will then settle and the reservoir will be refilled due to the firing of the main engine. Propellant Management Devices (PMDs) provide mission flexibility by allowing quick engine start-ups. It is compared to a hot gas system a simple system with passive components. Less complexity and passive parts will lead to more reliability. Important is also the cost saving aspect when a secondary propulsion system is not needed for pre-acceleration. Additionally the costs for flight system software will be reduced. The use of a capillary or surface tension device (PMD) to trap propellants over the outlet in low gravity is a more advanced, but especially for cryogenic liquids in Europe less understood technique. The technique is usable e.g. for Ariane 5 ESC-B like upper stages, either for reusable or non-reusable launchers, if a restart of the main engine is required.

A combination of both techniques is possible.

The main acceleration of upper stages is directed in direction of the main axis. Thus, due to the size of the propellant tanks of upper stages it is advantageous to use "partial retention PMD tanks". These tanks accommodate only a small amount of propellant at the outlet. Other types of PMD tanks are "total retention PMD tanks" and "compartment tanks". Total retention PMD tanks allow liquid control in the whole tank. This kind of tank is frequently used in satellites and in the future in the ATV. Compartment tanks are also used. They consist of two compartments.

The liquid in one compartment will be used for the main thrust firing. The other compartment's liquid will be used for attitude control [RD 2]. Fig. 2 shows a sketch of a partial retention PMD tank and the filling process of the reservoir which is located near the tank outlet at the bottom.
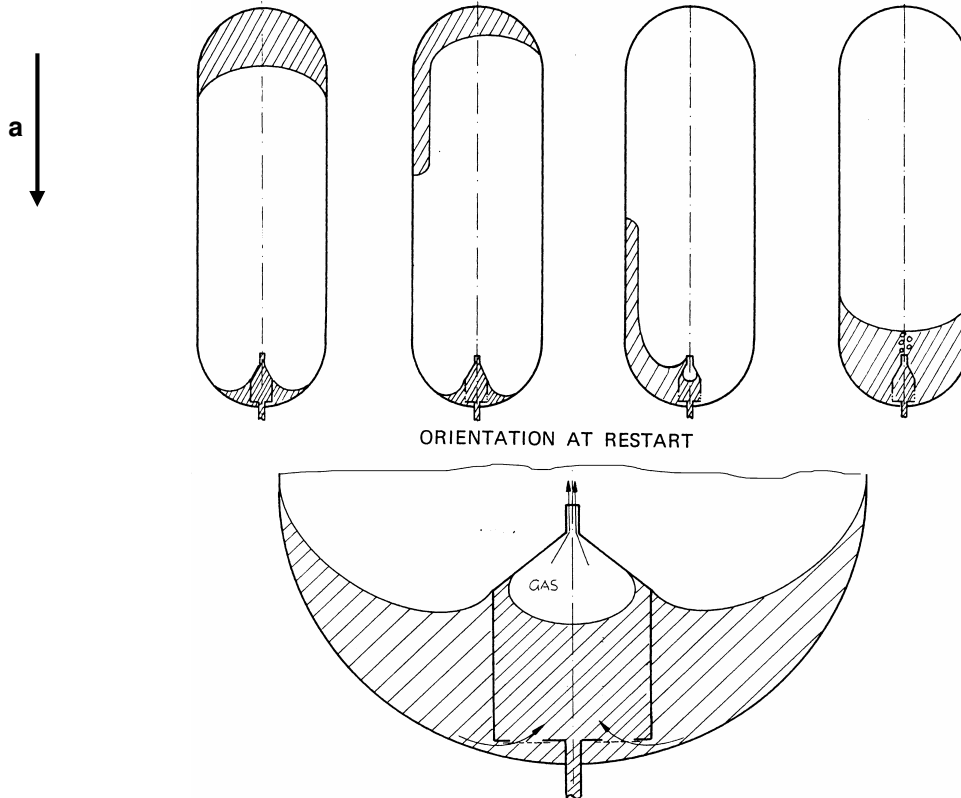

ORIENTATION AT RESTART

Fig. 2:   Re-filling of a reservoir in case of acceleration

The picture shows the filling process of the reservoir during longitudinal acceleration in the direction of the tank outlet. At the beginning of the re-orientation phase the bulk propellant outside the reservoir has been assumed as far from the outlet as possible. Thus the re-orientation time will have a maximum. The reservoir at the tank bottom will supply liquid to the engine while the propellant outside the reservoir re-orientates in the direction of the reservoir. The gas inside the reservoir will then be expulsed while the bulk propellant enters the reservoir. The reservoir will be re-filled (see also [RD 3]). The reservoir consists mostly of two housings. An example of a reservoir may be seen in the following picture.
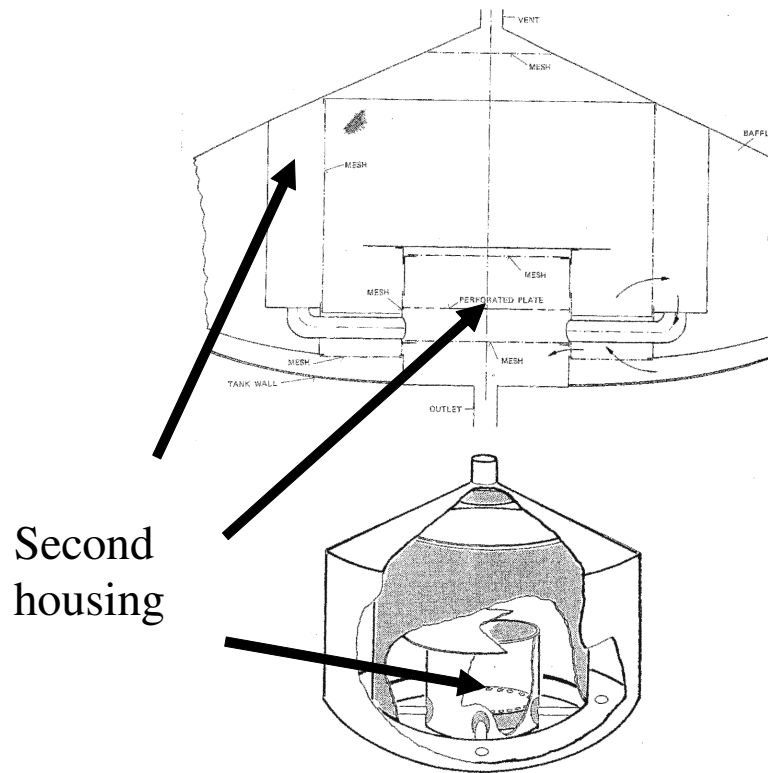
Second
housing

Fig. 3:   MBB / ERNO design of a PMD

The second housing will be placed directly in front of the outlet. Fig. 3 shows an example of a reservoir design with a second housing included into the reservoir. Screens attached to the housing allow the penetration of liquid. The penetration of gas is however prevented up to a certain pressure difference on both sides of the screens due to capillary effects. The pressure difference in case of gas penetration through a screen is called "bubble point pressure".

PMDs offer great advantages in case many restarts of the upper stage's main engine become necessary. One example is a mission to the ISS, such as the ATV mission. In case of ATV the PMD is used for reaction control and for main thrust to provide propellant in order to increase Δv.

PMDs enable greater flexibility since they are not limited with respect to the number of restarts. The enhanced restart capability of upper stages that use cryogenic propellants will improve their flexibility with respect to future missions. It is therefore anticipated to improve the knowledge and the CFD tools in order to improve the layout of this technique for the coming satellite and upper stage projects.

4.4.2 Application of PMD elements for upper stages

Upper stages with storable propellants

Many partial retention PMDs have been designed for upper stages which use storable propellants (e.g. Agena, Apollo [9]). The Ariane 5 upper stage EPS-V has also restart capability. The re-orientation of the propellant prior to re-ignition is enabled by the SCA system which will be also used for reaction control. Baffles have been introduced at the tank bottom above the tank outlet in order to reduce the sloshing motion of the liquid. A sketch of the baffles is presented in Fig. 4.
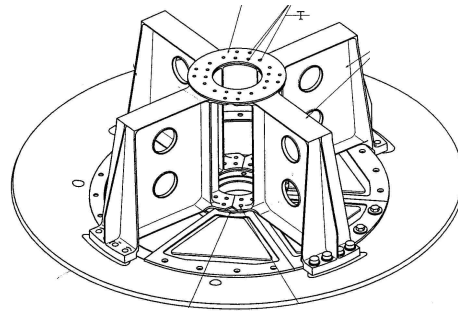
Fig. 4:   Baffle configuration above EPS tank outlet (GRD)

These PMD elements are very simple. However they effectively reduce the sloshing motion of the liquid. Thus the pre-acceleration time is reduced. As a result the consumed propellant mass by the SCA system is decreased [RD 4].

A more complex PMD is the total retention device used for ATV [RD 2]. The propellant is controlled in the whole tank (see Fig. 5). It is designed for continuous accelerations in all axes.
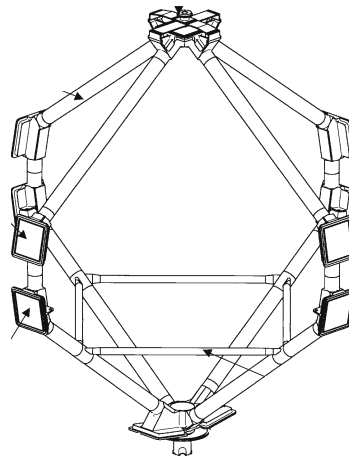

Fig. 5:   ATV PMD

The liquid is collected in a tube system and may penetrate the tubes through a number of pleated screens. The screens have been mounted close to the tank wall in the preferred 0g configuration of the liquid (see Fig. 6).
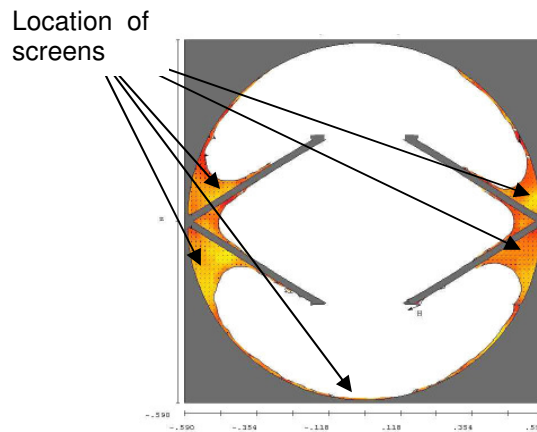
Location of screens

Fig. 6:   0g configuration in ATV tank

Conical baffles have been introduced in order to reduce the sloshing motion. In case of low fill levels the liquid will be located according to the picture above. A sufficient number of screens will be surrounded with liquid at all times.

Concepts for PMDs for cryogenic upper stages

PMD systems for cryogenic propellants impose additional challenges. Due to the low temperatures of the liquid and the heat input into the tanks nucleate boiling may occur especially in the LH2 tank during long coasting phases. Analyses concerning nucleate boiling have been performed e.g. by Colin [RD 5].

For small tanks the two-phase problem can be avoided by raising the pressure above the point of transition between liquid and gas (also known as the critical pressure). This system is used for storage and supply of hydrogen and oxygen for the shuttle power reactant supply and distribution system. Unfortunately this technique is not applicable for propulsion stages since the required pressures are too high [RD 6]. One concept for propellants that can be pressurized with its own vapour (such as oxygen and hydrogen) is to chill down the liquid in the tank. A quantity of cryogen is vented overboard. Boiling will then lead to a subcooling of the liquid.

The chilldown phase will have to be performed a sufficient time prior to engine ignition in order to ensure that all the vapour has condensed in the sub-cooled liquid and to ensure that the PMD has collected a sufficient amount of propellant.

In order to choose a suitable PMD concept for cryogenic upper stages a comparison has been carried out with the concepts described in the available literature. PMD concepts for cryogenic upper stages have been analyzed e.g. by Blatt [RD 7] in the frame of Centaur D-1S. These concepts have been compared to investigations carried out in the frame of ESC-B. In the following ESC-B will be used as a leading configuration, either as an upper stage for a dispensable rocket or as an upper stage of a reusable rocket / hopper.

According to Blatt [RD 7] the following candidate systems have been recommended:
1. Start baskets - refilled by settled fluid
2. Capillary device - refillable by pumping
3. Start tank with bypass feed system

Blatt [RD 7] points out that passively cooled start baskets appear to be the most promising capillary acquisition systems. Cooling coils required for active cooling result in an excessive weight penalty when designed for worst case condensation heat transfer. Thermal subcoolers appear to have substantial hardware weight and equivalent payload weight advantage compared to helium pressurization. Thermal subcoolers (heat exchangers using throttled cooling fluid to cool the fluid flowing to the boost pump) were the most promising subsystem analyzed in his study. A pumping system for returning coolant to the tanks, while adding complexity, offers the advantage of reduced weight and sharply reduced payload penalty sensitivity to the number of engine burns and total mission time.

4.4.3 Critical points based on the anticipated developments

Based on the assessment of the current status with respect to the anticipated developments a list of critical points has been derived. These points were used as a guide line for the COMPERE work. The evolved critical points are summarized in the following. The critical points were assessed and summarized by the COMPERE expert group prior to initiation of the COMPERE project. During the course of the project this list has been updated in order to take into account recent developments and findings in the frame of the project.

Propulsive phase:
1. Sloshing, non linear effects, initiation of break-up
2. Anti slosh ring
3. Formation of droplets
4. Vaporization of droplets due to thermal effects or/and concentration
5. Heat and mass transfer at interface and walls
6. Thermal stratification in draining phase

Engine shut-down:
1. Amplification of sloshing including geometric effects
2. Heat and mass transfer at interface and walls
3. Droplet and bubble formation by break-up
4. Vaporization of droplets due to thermal effects or/and concentration

Ballistic phase:
1. Location of the liquid within the tank, interface liquid/gas
2. Characteristic Time of damping for sloshing
3. Heat and mass transfer at interface and walls
4. Boiling, natural convection, Marangoni convection and thermal stratification
5. Dilution of gas into liquid phase
6. N2O4 chemical decomposition
7. Gortler instability (in relation with change of spin)

Preparation of engine restart:
1. Geyser formation, liquid fragmentation, inclusion of gaseous bubbles, outgasing time, settling time
2. Heat transfer at the wall in connection with fluid rising at the walls
3. Heat and mass transfer due to de-pressurization and pressurization
4. Draining for chill-down
5. Rising of bubbles due to chill-down

5. Performed Work

5.1 Logic of performed work

Goal of the COMPERE project is to analyze the critical points summarized in the previous chapter. In most cases the different phenomena will occur in a coupled manner which means that in cryogenic stage tanks thermal effects, reorientation effects and sloshing phenomena will for example occur in combination. To simplify the treatment of the different phenomena the different physical aspects have been analyzed separately in a first series of benchmark tests (see Fig. 7). These benchmark tests include analyses concerning:

➢ Sloshing of propellants in tanks
➢ Reorientation from high to low acceleration
➢ Thermal stratification
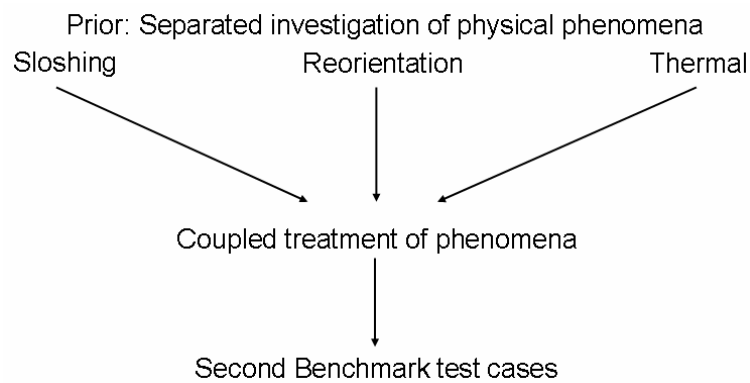

Fig. 7:   Investigation logic concerning the COMPERE project

A second series of benchmark tests (including analyses) then treats the coupled phenomena such as non-isothermal reorientation.

An overview of the different analyses carried out will be given in the following chapters.

5.2 First Benchmark Test Cases

5.2.1 Test Case 1: Sloshing in a rotating tank (3D)

The aim of this benchmark test case was to study the ability of numerical codes to reproduce the sloshing of a liquid in a rotating tank at high Froude number and high Bond number (surface tension effects can be neglected compare to gravity and inertial forces). The benchmark was three dimensional and the experimental data were provided by Astrium in collaboration with ZARM in the frame of the EPS upper stage development.

A sketch of the test setup and the model tank used for the experiments can be seen in. The model tank consists of a hemispherical bottom and a cylindrical upper compartment. The upper hemispherical part of the original EPSV tank is not required for the experiments and has been thus omitted. Just about all tests were carried out with a constant spin rate. The picture shows the initial liquid position as confined by the liquid release device and the stable liquid position after the fluid's settling. The tests were carried out for different filling levels.
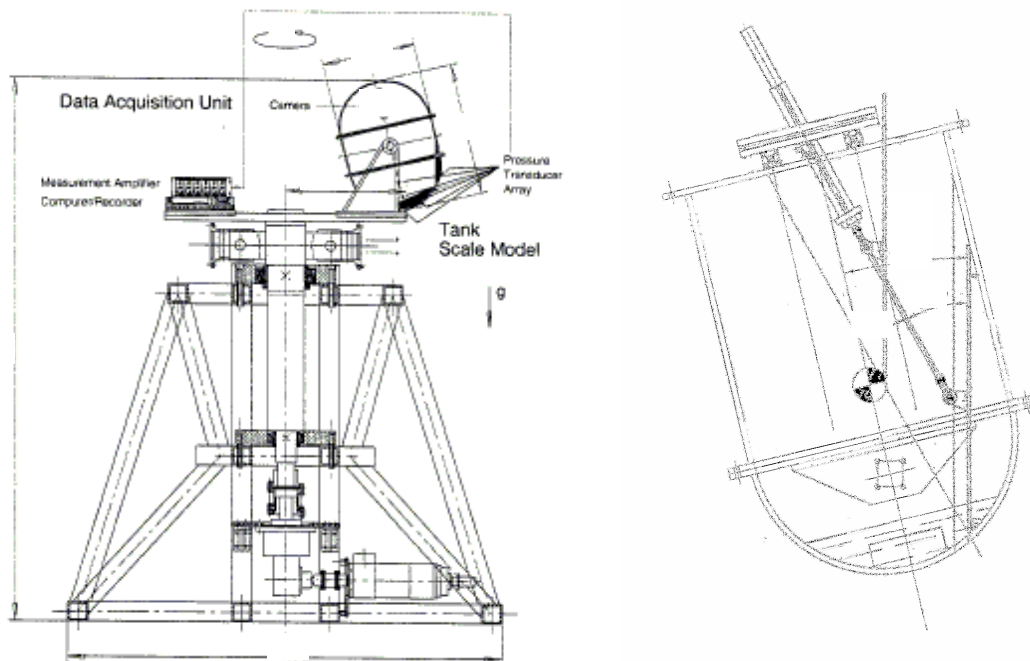

Fig. 8:   Principle of experiment setup and detail of model tank

For the evaluation of the sloshing frequency and the damping of the experiments as well as comparisons with respective data from numerical simulations, three independent systems were used:
- Video observation
- Pressure measurement
- Force measurement

Video observation was used to get a rough impression of the liquid motion inside the tank. The single frames were compared to FLOW-3D plots. Pressure sensors were placed at distinct points on the GRD. They provided local data. From the force data the position of the liquid's centre of mass can be calculated.

Two tests were carried out with different fluids:
  ➢ Test number 1: SF-0.65
  ➢ Test number 2: water.

A view of the geometrical conditions inside the test tank is shown in Fig. 9.
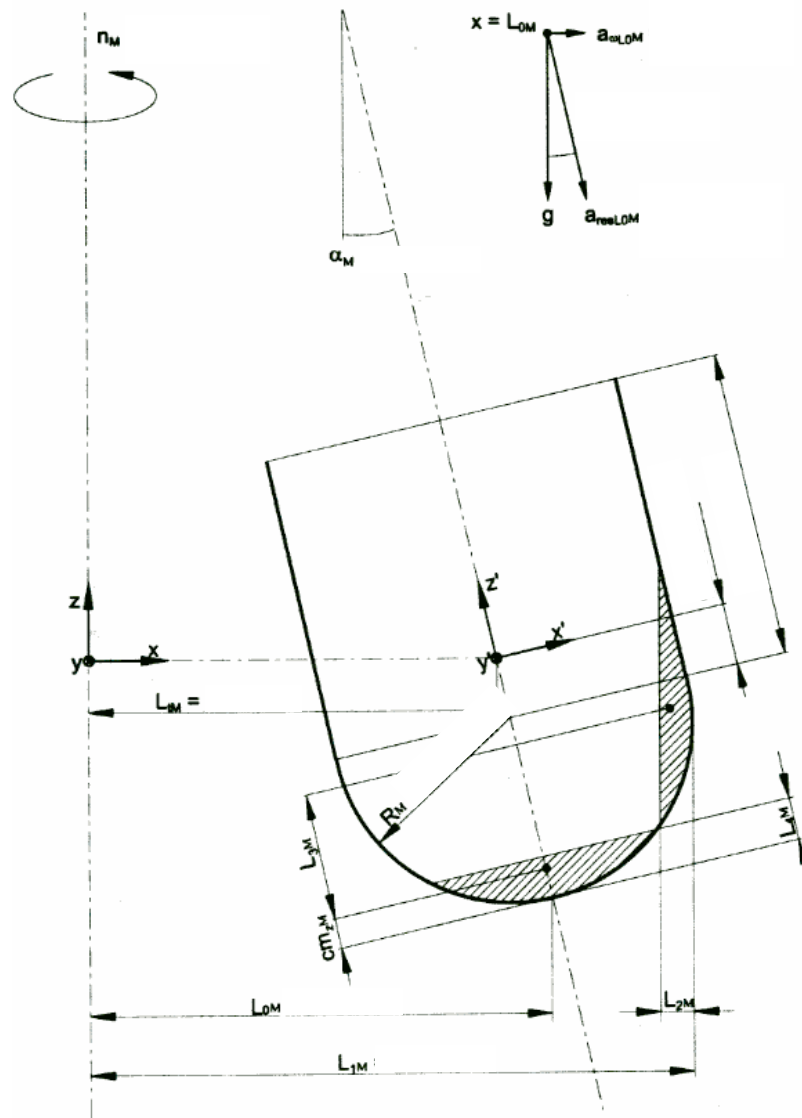
Fig. 9: Initial and final condition of the liquid inside the test tank

FLOW-3D analyses have been carried out at Astrium in Bremen in order to validate the code with the available data set. The initial condition for the numerical model, similar to Fig. 9, is shown in Fig. 10.

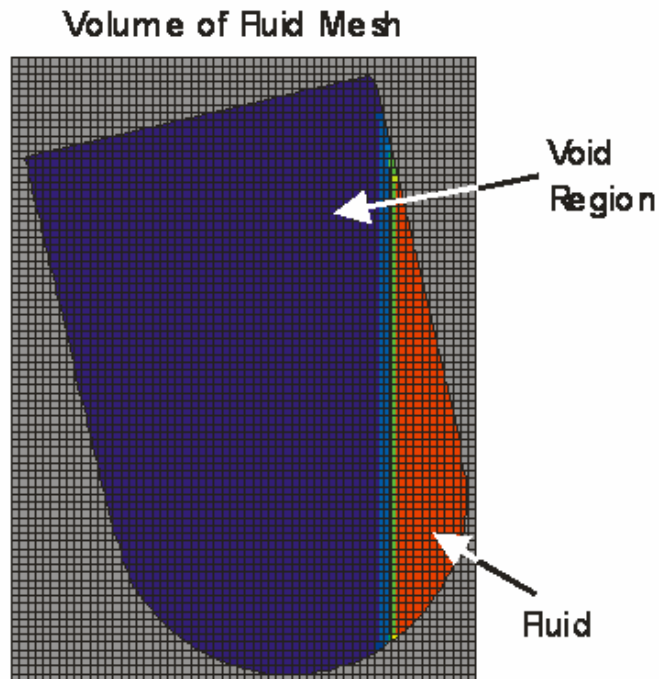### Volume of Fluid Mesh

Fig. 10:   Initial condition for numerical model (60x50x80 mesh)

At that time FLOW-3D version 7.7 was used for the evaluation. A summary of certain parameters with respect to the model are given below:

Physical aspects:
> ➢ Incompressible fluid
> ➢ Laminar viscous flow
> ➢ Wall shear considered
> ➢ Constant surface tension
> ➢ 0° contact angle

Numerical aspects:
> ➢ Finite Difference Algorithm
> ➢ Volume of Fluid model
> ➢ Monotonicity Preserving 2nd Order Method
> ➢ Fluid fraction of each cell calculated
> ➢ Rectangular equidistance grid cells (60x50x80 mesh)
> ➢ Implicit pressure iterations using the SOR method
> ➢ Explicit viscous stress evaluation
> ➢ Time step range: 2.0e-8 s < Δt < 0.04 s

Fig. 11 shows results obtained from the FLOW-3D simulation for different times.
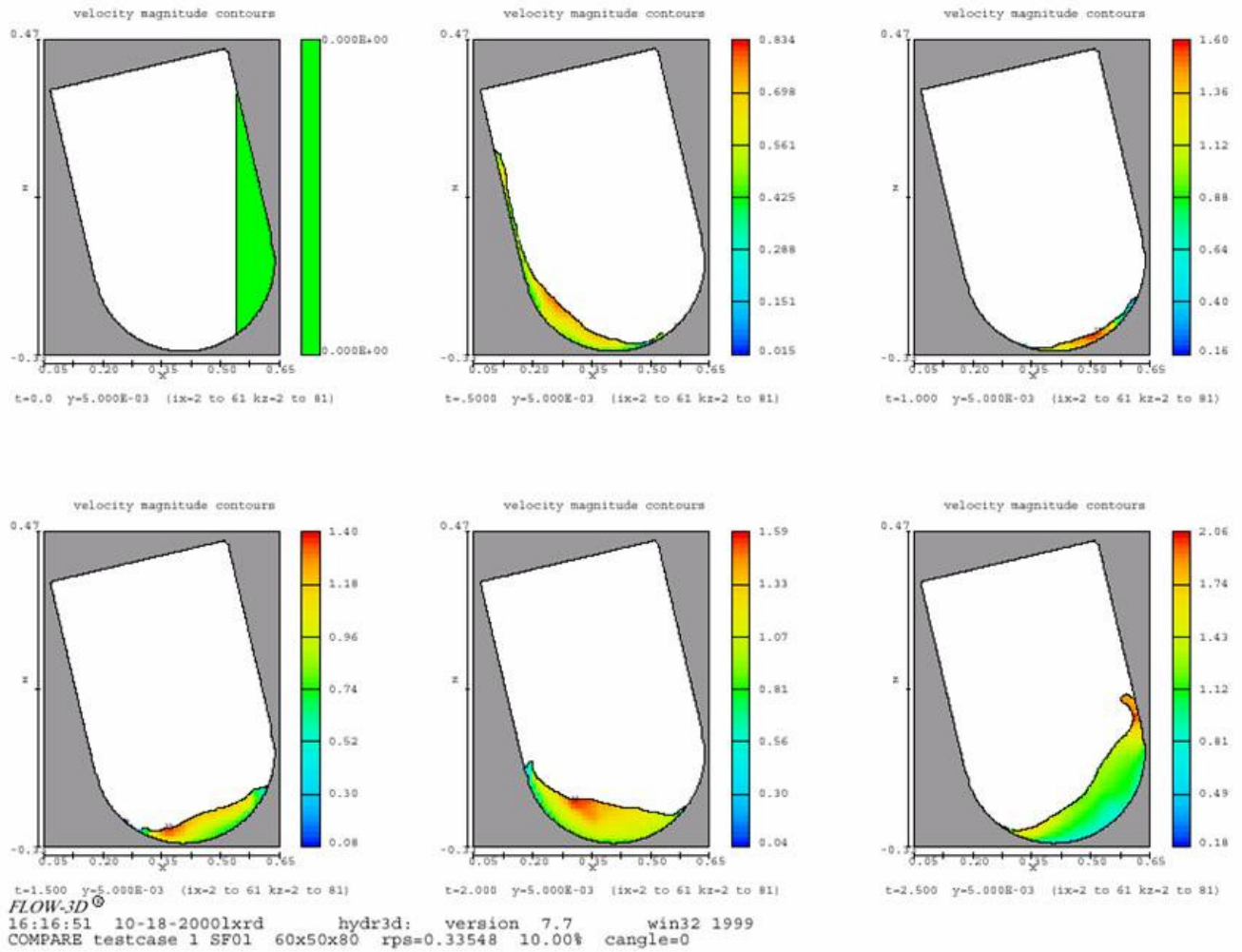
Fig. 11:   Results obtained from the FLOW-3D simulation for different times

A comparison of the experimental data and the numerical computations of the pressure at the probe has been carried out by ONERA estimating the L2 relative Error (energy norm) between the experimentally obtained pressures (measured at 5 probes located on the bottom of the vessel) and the numerical results. The software codes Eole, FLOW-3D, FLUENT and Fluidyn were considered in the benchmark analysis. The results of the benchmark analyses are given in the following table:

	Eole	FLOW-3D	FLUENT	Fluidyn
Test 1	.6308	.6547	.5095	.5857
Test 2	.4822	.3259	.2735	.6954

Table 1:   ONERA evaluation of the test case 1 with respect to the software codes Eole, FLOW-3D, FLUENT and Fluidyn

The four codes gave good results. Best solutions were obtained with FLUENT, then FLOW-3D, Eole and finally Fluidyn.

The following conclusion can be made with respect to the critical aspect of sloshing modelization:
  ➢ The non-linear forced sloshing amplitudes as well as wave breaking conditions and breaking mechanisms near resonant forcing have been clearly identified. The boundaries of transition to a swirling

mode have been determined. Expressions for the characteristic times of the growth in wave amplitude are given.

➢ When the forcing is stopped, the sloshing motion is shown to decay exponentially in time with a 1/e fall-off in about 40 periods for large fill ratio. This time decreases with decreasing fill ratio. An anti-slosh ring, when correctly positioned, decreases the damping time by about a factor of 30.

➢ The results concerning the drop sizes which result from wave breaking are still preliminary. The complexity of the liquid surface topology and the different mechanisms at the origin of drop formation make the determination of the drop sizes related with sloshing near the first asymmetric mode difficult.

As a conclusion sloshing analyses in the frame of upper stage tanks to estimate the sloshing forces are possible with the tested software, especially FLOW-3D and FLUENT. In order to be more confident in the accuracy of force and torque computation, complementary numerical work is necessary.

The results of this benchmark test were directly applicable for the validation of the EPS upper stage configuration, i.e. the determination of the settling times. Under consideration of the results of this benchmark test case the additional baffles were included in the EPS tanks. Fig. 12 presents a sketch of the chosen baffle solution mounted on the GRD.
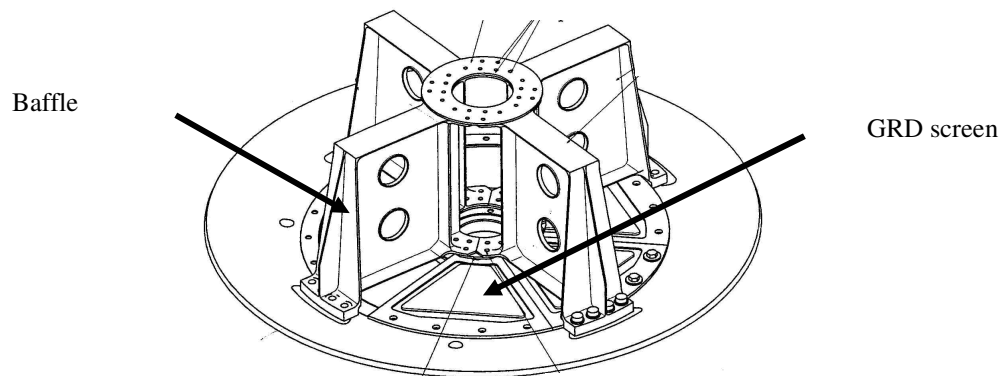

Fig. 12:   Sketch of the chosen baffle solution mounted on the GRD

5.2.2 Test Case 2: Sloshing in a two dimensional wedge

This test case aims to study the ability of numerical codes to reproduce accurately the sloshing of a liquid in a two dimensional wedge. Two sub test cases were performed: the first one at a low Froude number corresponding to linear oscillations of the free surface and the second at a high Froude number corresponding to large motions of the liquid. Surface tension effects as well as damping due to viscosity forces are neglected (high Bond and Galileo numbers). The tests were carried out with water. The geometrical conditions are depicted in Fig. 13.
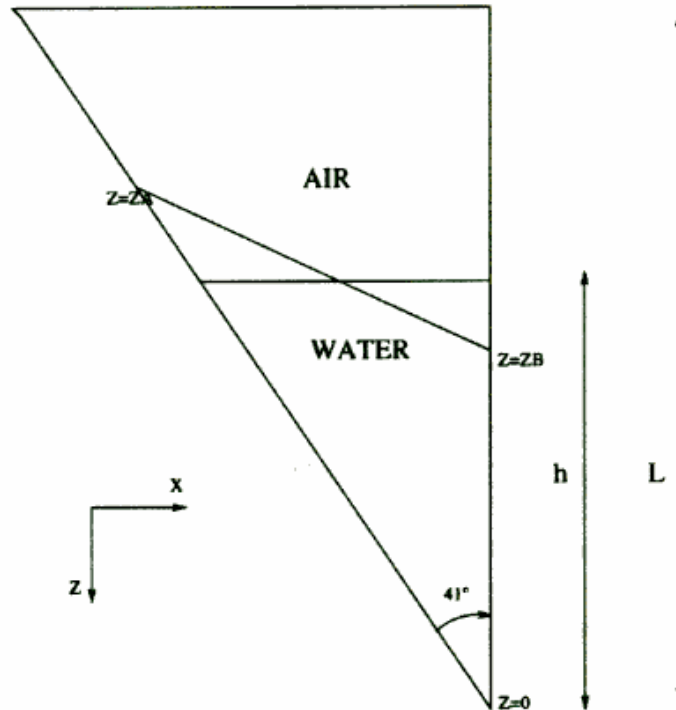

Fig. 13:   Geometrical conditions of test case 2

The experiments were performed at ZARM, choosing the following parameters:
- Test one with a horizontal acceleration $a_x = 0.981$ ms^{-2} and a high filling ratio (h/L)
- Test two with a horizontal acceleration $a_x = 9.81$ ms^{-2} and a low filling ratio (h/L).

At Astrium FLOW-3D analyses were carried out in order to compare the two test cases with the experimental results. The applied physical and numerical conditions are listed below:

Physics:
- Incompressible fluid
- Laminar viscous flow
- Wall shear considered
- Constant surface tension considered

Numerics:
- SF0.65, ax=0.981m/s2:150x150 cells
- FC77,   ax=9.81m/s2: 300x300 cells
- Explicit viscous stress evaluation
- Implicit pressure iterations using the SOR method
- Time step range: $0.00000001s < \Delta t < 0.01$ s

A series of plots from the FLOW-3D analyses for tests number 1 and 2 are given in Fig. 14 and Fig. 15.

COMPERE

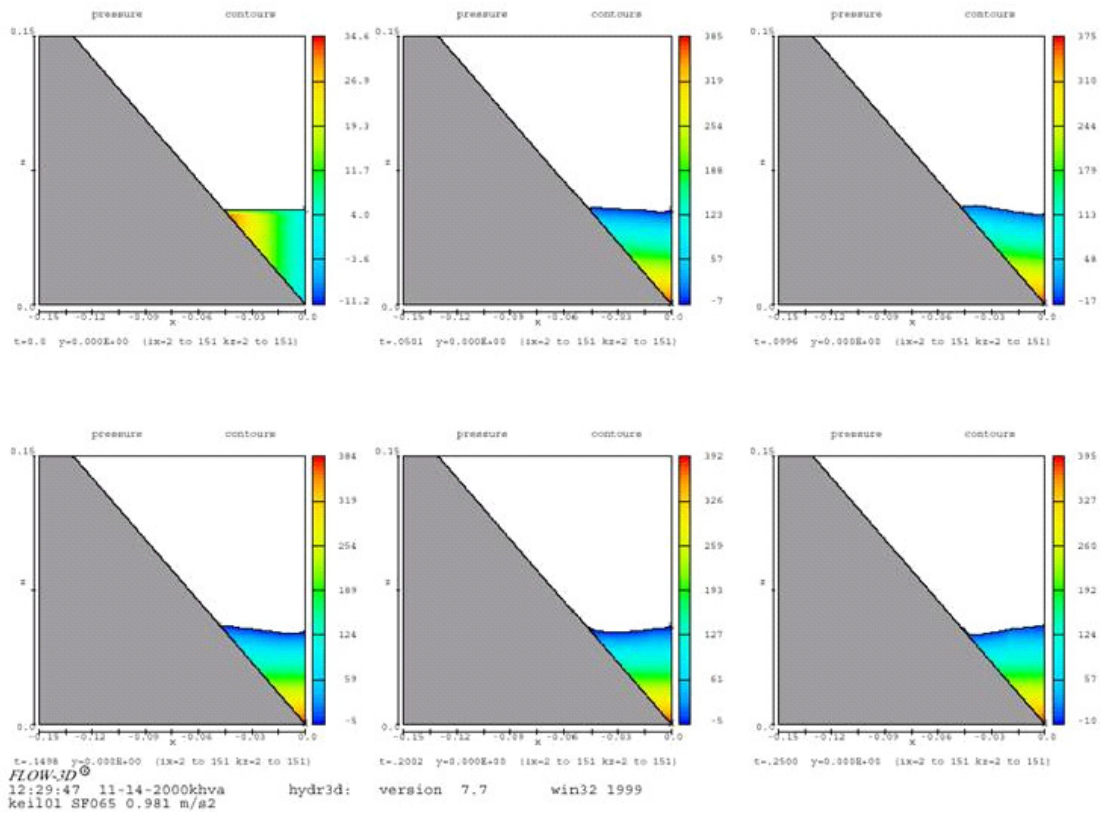| Dok.Nr./No.:	TE51-RIBRE-TN-0067		
Ausgabe/Issue:	1	Datum/Date:	15.06.07
Seite/Page:	21	von/of:	67

Fig. 14:   Results of test number 1 obtained from the FLOW-3D simulation for different times
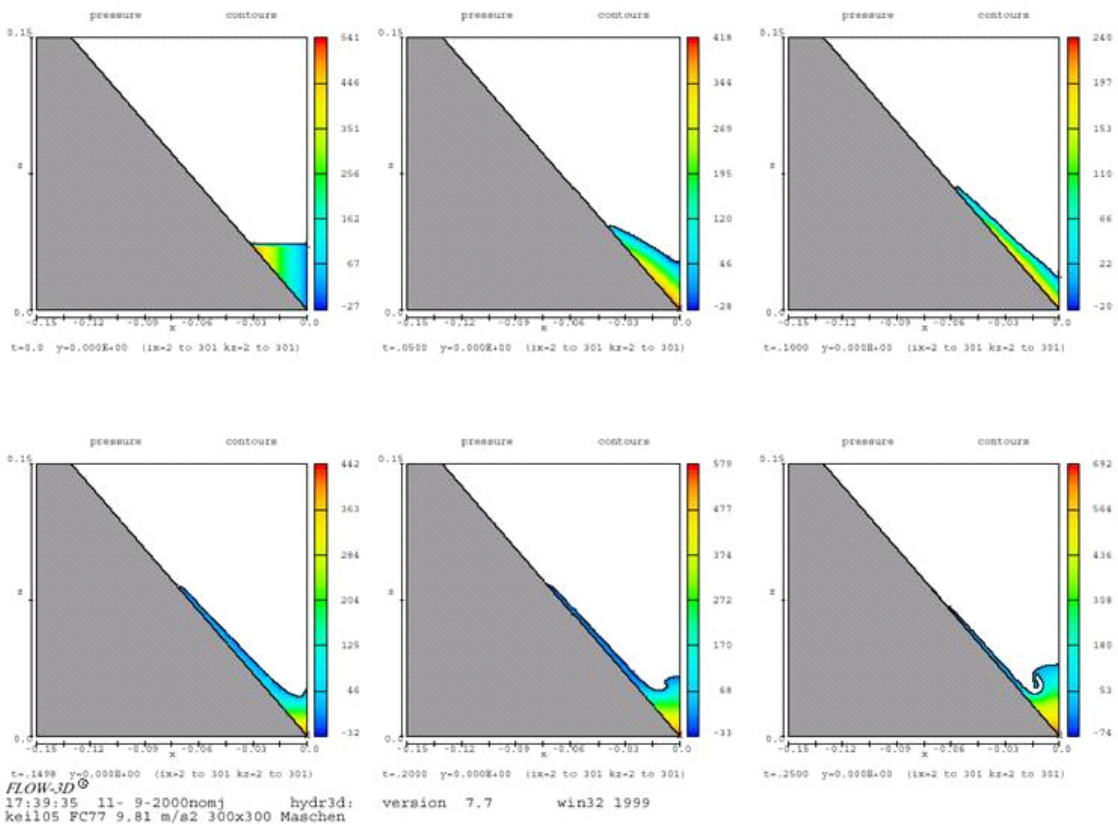

Fig. 15:   Results of test number 2 obtained from the FLOW-3D simulation for different times

Comparisons of the time history data for the experimental and the numerical results were performed for the hydrostatic heights at the vertical wall section (right) and at the wedge (left). The L2 relative error (energy norm) between the experimental value and the numerical results has been computed (see Table 2). The software codes Eole, FLOW-3D, FLUENT and Fluidyn were considered in the benchmark test case.

	Eole	Flow3D	FLUENT	Fluidyn
Test 1	.66	.54	.28	.76
Test 2	.26	.136	.20	.39

Table 2:   ONERA evaluation of the test case 2 with respect to the software codes Eole, FLOW-3D, FLUENT and Fluidyn

The best results were provided by FLUENT, then FLOW-3D. Eole also gave good results. Results of Fluidyn were too much damped and gave a poor precision.

As a general conclusion concerning this test case the following statements can be given:
- ➢ The FLOW-3 software, as used by Astrium, proved to be suitable to assess this kind of wave breaking phenomena.
- ➢ The test case enabled a good understanding of the liquid behaviour and the breaking process under idealized conditions. The breaking process is complex and it is therefore difficult to establish a simple relation for the drop size or / and the interfacial area, especially when considering the limited resolution of the numerical analyses. Concerning future assessments it will be therefore necessary to focus especially on wave breaking, gas entrapment into the liquid and vibration aspects. This would require a test case with more realistic geometries and force conditions.

5.2.3 Test Case 3: Reorientation after a step reduction of gravity

The aim of this test case was to study the ability of numerical codes to compute the reorientation of a free liquid surface in an axis-symmetrical container after a sudden reduction of the gravity. Two subsets were defined. In the two cases the flow is dominated by capillary effects. The Bond number varies from 100 to 0 and the Weber number is in the order of one. The tests were carried out under isothermal conditions. Thus any thermal effects were neglect.

Only three codes (FLUENT, FLOW-3D and Eole) have provided realistic results. The fluids used in the subtest 1 was "DEDRA" with a static contact angle of 5° and "M3" with a static contact angle of 55°. Numerical tests were performed with fixed contact angle. FLOW-3D however also uses a dynamic contact angle model which enables an adaptation of the contact angle as a function of the velocity of the contact line. The geometrical condition of the fluid at the end of the reorientation process is shown in Fig. 16.
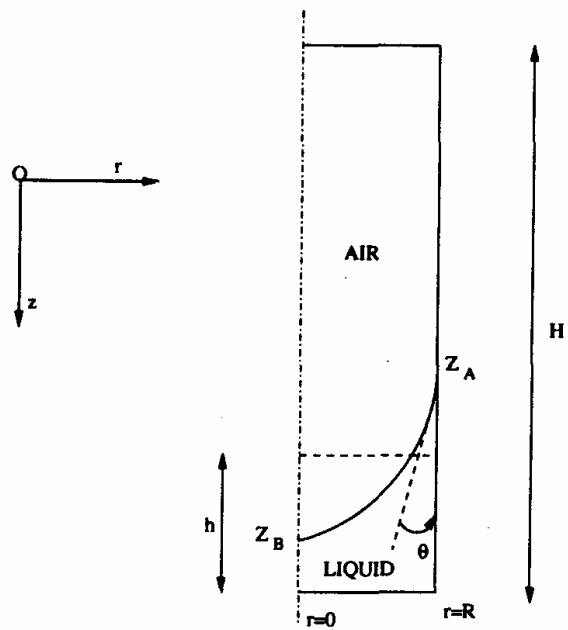

Fig. 16:   Geometrical condition of the liquid at the end of the reorientation process

In contrast to the other codes the FLOW-3D computations were carried out with a three dimensional model which allowed a more realistic comparison with the reorientation cases occuring in satellite and stage tanks.

The physical and the numerical conditions of the FLOW-3D simulation are depicted below:
Physics:
  ➢ Incompressible fluid
  ➢ Laminar viscous flow
  ➢ Wall shear considered
  ➢ Constant surface tension considered

Numerics:
  ➢ Equidistant mesh
     o DETRA (5.5° static contact angle)   25x25x250 cells
     o M3   (55° static contact angle):   50x50x130 cells
  ➢ Implicit viscous stress evaluation
  ➢ Implicit pressure iterations using a line implicit method
  ➢ Time step range: 1.0e-8 s $< \Delta t <$ 0.047 s

A view of the reorientation process for DETRA (5.5° static contact angle) and M3 (55° static contact angle) is shown in Fig. 17 and Fig. 18.
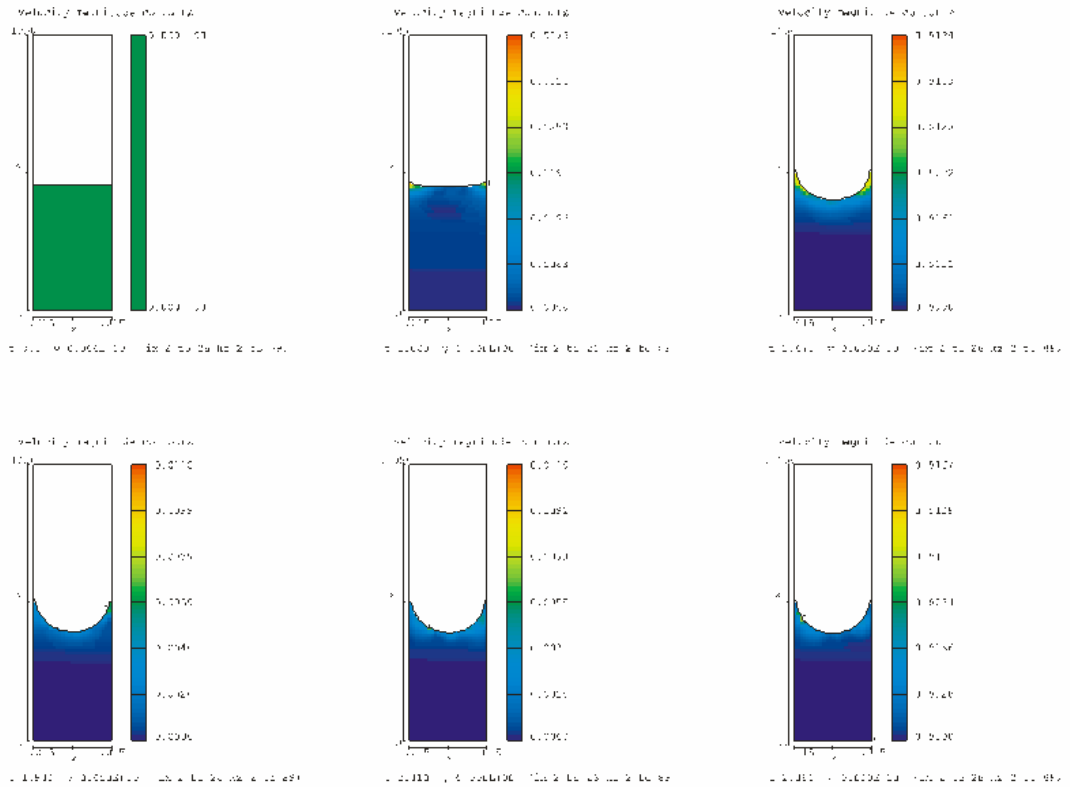
Fig. 17: FLOW-3D plots of the reorientation process with DETRA (5.5° static contact angle) at different times during reorientation
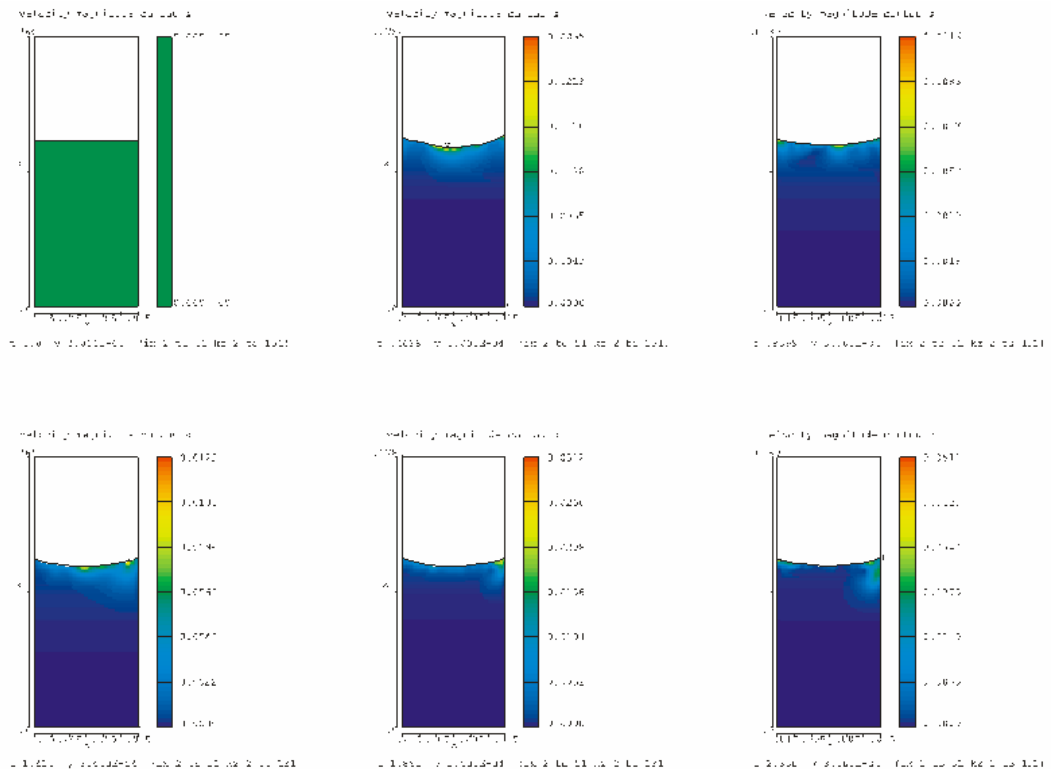

Fig. 18: FLOW-3D plots of the reorientation process with M3 (55° static contact angle) at different times during reorientation

For the analysis the centre point z_A as well as the motion of the contact line z_B were monitored and compared with the experimental results. The following table gives the L2 relative error between the experimental values of z_A, z_B and the computed values.

	Eole	FLOW-3D	FLUENT
Test 1 (Detra) z_A	.39	.52	.44
Test 1 (Detra) z_B	.42	.83	.14
Test 2 (M3) z_A	1.42	.51	.07
Test 2 (M3) z_B	.64	.44	.2

Table 3:   L2 relative error between experimental values and numerical results of z_A and z_B for tests 1 and 2

The accuracy of FLUENT results was very good. FLOW-3D results were qualitatively good, but not as accurate as the FLUENT results since a 3D mesh was used which results in a much coarser numerical mesh. However the accuracy proved to be sufficient in order to be used for upper stage and satellite functional analyses. A number of 2D analyses were furthermore carried out which proved that the accuracy with respect to the experimental results is excellent if the grid resolution is high enough. Eole results were of very poor accuracy.

Calculations comparable to this benchmark were carried out in numerous cases for the layout of upper stages and satellites. As an example the 0g configuration inside the OST-4 Propellant Refillable Reservoir (PRR) is given in Fig. 19.
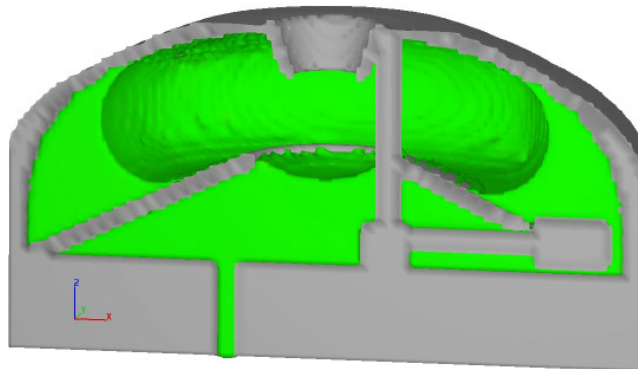

Fig. 19: OST-4 PRR FLOW-3D simulation

The present analysis states the location inside the PRR during refilling after an expulsion process. Most cases require a 3D numerical model in order to be representative. Verification of the code's accuracy for this case was therefore of special interest.

5.2.4 Test Case 4: Modelling of stratification inside closed LH2 tank

This test case concerns the study of thermal stratification inside a closed LH_2 tank maintained at constant pressure (5 bars). The experimental results were provided by Air Liquide. The tank was filled with liquid hydrogen. Heat input into the tank will result in a stratification process. The temperature history profile at certain points along the tank's centre line was plotted.

The numerical modelizations only considered the liquid phase. Initially a uniform temperature distribution, corresponding to the saturation temperature of LH_2 at 5 bars, was prescribed. The geometrical conditions of the test tank are shown in Fig. 20.
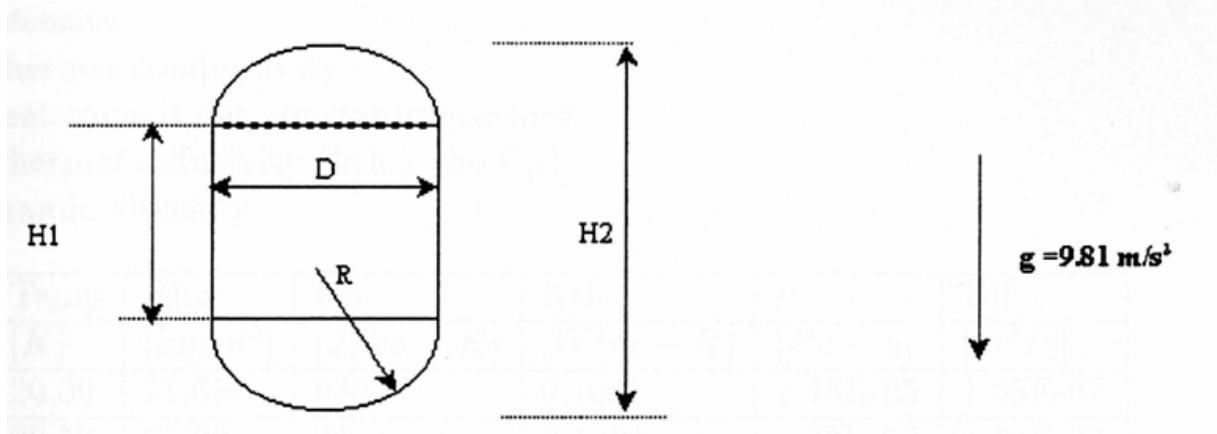

Fig. 20: Geometrical conditions of the test tank

The experimentally measured temperature profiles were provided by Air Liquide for five different subtests. For each subtest a different heat flux was applied on the cylindrical part and the lower bulkhead of the container. FLOW-3D analyses were carried out at Astrium considering the following conditions:

Physics:
  ➢ Energy equation with full momentum equations and heat transfer
  ➢ Incompressible fluid with void gas region
  ➢ Temperature dependent laminar and turbulent viscous flow, heat capacity and density
  ➢ Wall shear considered
  ➢ Constant surface tension considered (not relevant since high Bo number test)

Numerics:
  ➢ Equidistant mesh 15x15x45 cells
  ➢ Implicit viscous stress evaluation
  ➢ Explicit heat transfer
  ➢ Implicit pressure iterations
  ➢ (SOR method)
  ➢ Influence of void region not considered
  ➢ Time step range: 1.0e-8 s < Δt < 0.01 s

The observed reorientation and stratification process is shown in Fig. 21. The left picture shows schematically the vortices which will form inside the liquid and the ullage due to the thermal convection process.
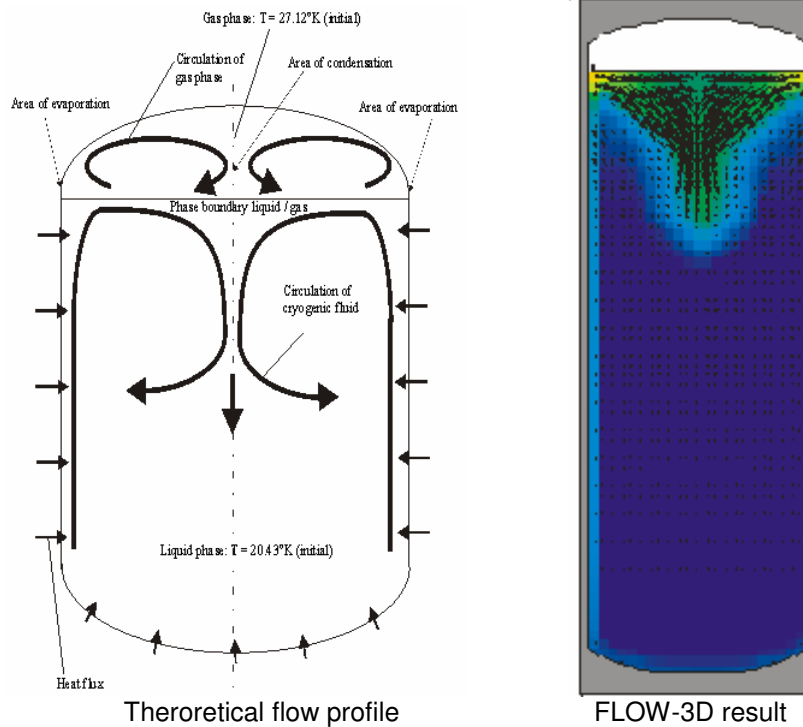
Theroretical flow profile   FLOW-3D result

Fig. 21:   Reorienation of the liquid inside the test tank due to thermal heat fluxes through the tank's side walls into the liquid

Best results were again obtained with the FLUENT software. FLOW-3D results were less accurate since a 3D geometrical mesh with coarser grid cells was chosen. It should be however be noted that the 3D results are much more realistic with respect to the real applications within upper stage tanks. A summary of the L2 relative errors for the different codes, here for subtest 4 (external thermal flux of 137 W) is plotted in Fig. 22.
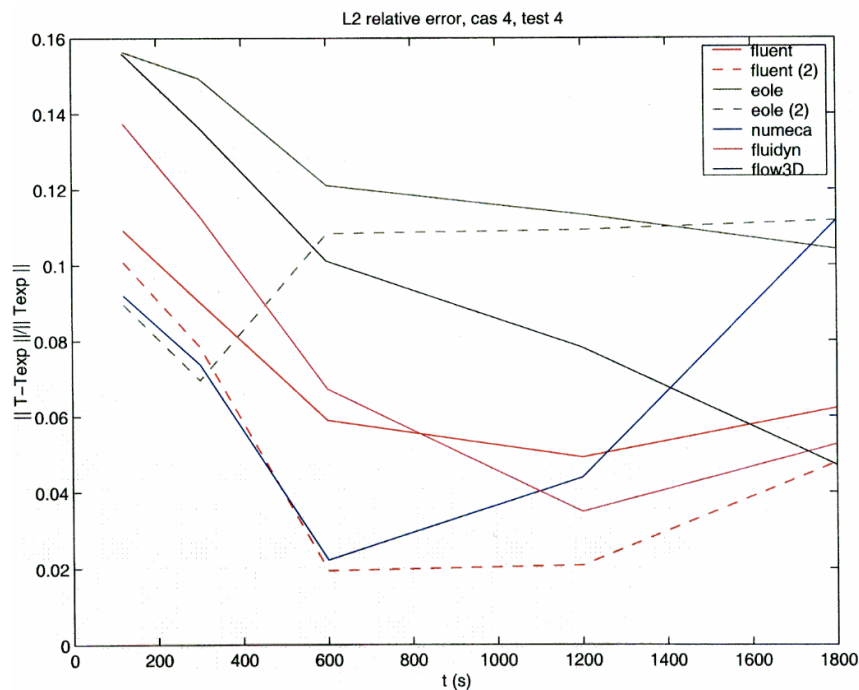

Fig. 22:   Summary of the L2 relative errors for the different codes (FLUENT, FLOW-3D, NUMECA, FLUIDYN, EOLE), here for subtest 4 (external thermal flux of 137 W)

It should be noted that the numerical grid of the present numerical analyses with FLOW-3D is very coarse (15x15x45 mesh). Finer grid resolutions will improve the accuracy of the results considerably. Due to increased computer power since the time the calculation was carried out, the amount of mesh cells the computer system can handle, has also grown. Presently calculations up to 1 million cells can be handled. For comparison: the present FLOW-3D calculation was carried out with 10125 cells. This is almost a factor 100 less.

An example for an upper stage application with respect to thermal stratification is shown in Fig. 23.
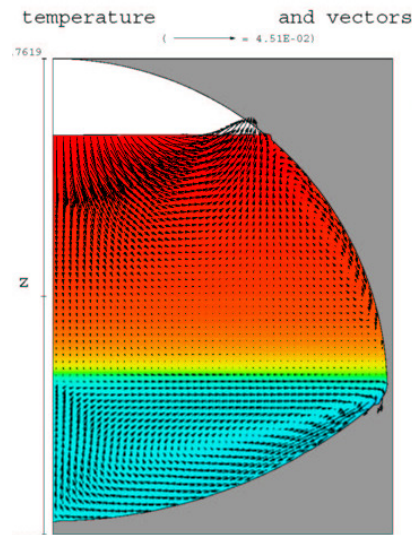

Fig. 23:   Thermal stratification inside ESC-B LOX tank on ground due to heat transfer through the tank walls

In this case heat losses through the upper tank shell towards the adjacent LH2 tank and heat input through the lower tank walls lead to a stratified temperature layer as shown in Fig. 23. Analyses of this kind are required to estimate the temperature history inside the tank.

5.2.5 Conclusion from first benchmark test cases

The performed first benchmark test cases showed that the FLOW-3D code is well able to carry out numerical analyses concerning the following phenomena:
- Sloshing
- Reorientation
- Stratification

With respect to sloshing the higher sloshing damping of the numerical calculation has to be taken into account. Assessment of droplet formation is still difficult since the numerical mesh is generally too low to detect them. Alternative models, e.g. by modelling the droplets as particles could be an alternative. These kind of features are available in the FLOW-3D code.

Generally the accuracy of the numerical results has improved considerably since the time when the calculations were carried out. Main improvement is the increased computer power. Thus it can be expected that today the same calculations will lead to much improved results. This tendency was also observed in the frame of newer benchmark analyses. The benchmark test cases should be therefore repeated from time to time in order to keep track with the changes within the software and the computer power.

5.3 COMPERE Propellant Tank Simulation Software (COMPTAS)

Within the COMPERE Project, a propellant tank simulation software (COMPTAS) has been established as engineering S/W tool. COMPTAS shall be used for the analysis of the behaviour of fluids (liquids and gases) in a tank for different gravity conditions simulating all major physical processes for fluid inflow / outflow, phase change, heat transfer, fluid mixing and gravity events (fluid sloshing, re-orientation, settling, geysering).

The COMPTAS software user requirements cover propellants, pressurant, tank configurations, analytical performance, nodal discretisation, accuracy, S/W environment, validation and delivery. The S/W environment for COMPTAS has been selected with EcosimPro.

The tank is shown as a cylindrical tank schematically in Fig. 24. The tank consists of the structure (wall, top and bottom), the insulation (wall top, bottom), the fluids (fluid, gas), the fluid inlet ports (liquid, gas) and thermal ports at every external insulation surface.
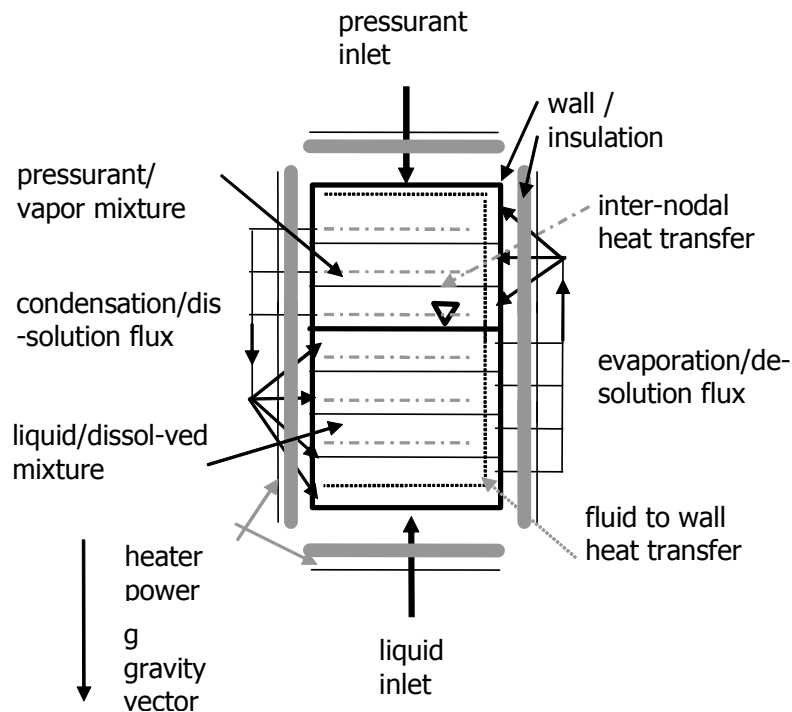

Fig. 24:   Overview of the COMPTAS model

The tank wall might be subdivided into *nw* lateral an *np* peripheral nodes, the fluid into *nl* liquid and *ng* gas nodes. The wall insulation is assumed to cover the *nw* wall nodes and the top and bottom nodes. The node numbering starts for the nl liquid nodes and the nw wall nodes from the bottom, for the ng gas nodes from the top. The default direction of the gravity vector is parallel to the tank axis and from top to bottom.

The set of nodes of the tank consists of structural and insulation nodes (walls, top, bottom) and fluid nodes (liquid, gas).

The interface with the environment is given by the fluid ports (here defined as inlets for liquid and gas) and thermal ports (here defined with specific heat flux or temperature for the outer insulation surfaces).

The node numbering schematic is for the wall/insulation nodes from bottom to top, for the propellant (at default gravity vector) from bottom up to the liquid/gas interface, for the gas from top down to the gas/liquid interface.

The first fluid nodes *#1* (liquid and gas) are directly linked to the respective fluid inlet ports.

Normally, the gravity vector is assumed in the direction parallel to the tank axis top to bottom, with the gas in the upper tank volume near the gas inlet port, and the propellant in the bottom part of the tank above the liquid inlet port.

In case the gravity vector changes the direction, always the fluid nodes are assumed to be separated by the gas/liquid interface plane normal to the gravity vector, with the last liquid node *nl* and the last gas node *ng* at the gas/liquid interface, and the first fluid nodes at the opposite structural interface.

The gas is actually considered as mixture of gas and vapour, with common total pressure, but different partial pressures in the different gas nodes according to the mass fractions of the gas/vapour mixture constituents.

In the following, "gas" denotes the pressurant gas/vapour mixture, sometimes also labelled with "mix". "Fluid" means either liquid or gas; "liquid" means the liquid propellant/dissolved pressurant mixture.

In the gas, the properties are calculated using the commonly used mixture rules with mass/molar fractions of constituents. In the liquid, the contributions of dissolved pressurant to the properties are neglected.

The interface at the fluid ports is analyzed using total mixed mass/enthalpy flows together with the local mass fractions to take care of the correct mass/energy transfer and the correct transfer of the local gas/liquid constituents.

Fluid Re-Orientation/Settling

Liquid re-orientation takes place due to surface tension forces after a change of the effective gravity from high to low levels. The re-orientation velocity depends on the rate of change of effective gravity, the final effective gravity level, the liquid surface tension, the dynamic contact angle at the contact line of the liquid/gas interface with the tank wall, the internal tank geometry (protrusions, baffles, PMDs, sieves, etc.), and phase change effects at the wetted surfaces.

The final shape of a liquid with zero contact angle after re-orientation at zero gravity is characterized by the liquid covering the all-wetted tank wall with the free gas/liquid interface area minimized and the gas contained inside.

Liquid settling takes place e.g. after a non-zero effective gravity level at constant direction has been applied to the tank and the fluids have come to rest in a certain position fixed in relation to the tank wall, with the free surface according to the effective gravity level and the surface tension, forming a curved surface for surface tension-dominated modes, and a more or less flat free surface with a meniscus near the wall interface for effective gravity-dominated modes.

For COMPTAS, the modelling of liquid re-orientation / settling is planned to represent the re-oriented or settled mode under the following convention:
- the first liquid/gas nodes are always in contact with the liquid/gas inlet ports
- the last liquid/gas nodes are always in contact with each other
- the first gas node is for re-oriented conditions at zero effective gravity, zero contact angle and fully wetted tank wall in the centre of the gas volume, however still in artificial contact with the gas inlet port for numerical reasons
- the intermediate states between fully re-oriented and fully settled is to be simplified in terms of fluid/wall and fluid/fluid heat transfer areas and times of change of modes
- the characteristic time of change of modes between fully settled to re-oriented is calculated for zero effective gravity from the surface tension, the contact angle and the fluid/tank geometry
- the characteristic time of change of modes between fully re-oriented to fully settled is calculated for non-zero effective gravity from the effective gravity change, the fluid/tank geometry and a simplified momentum equations.
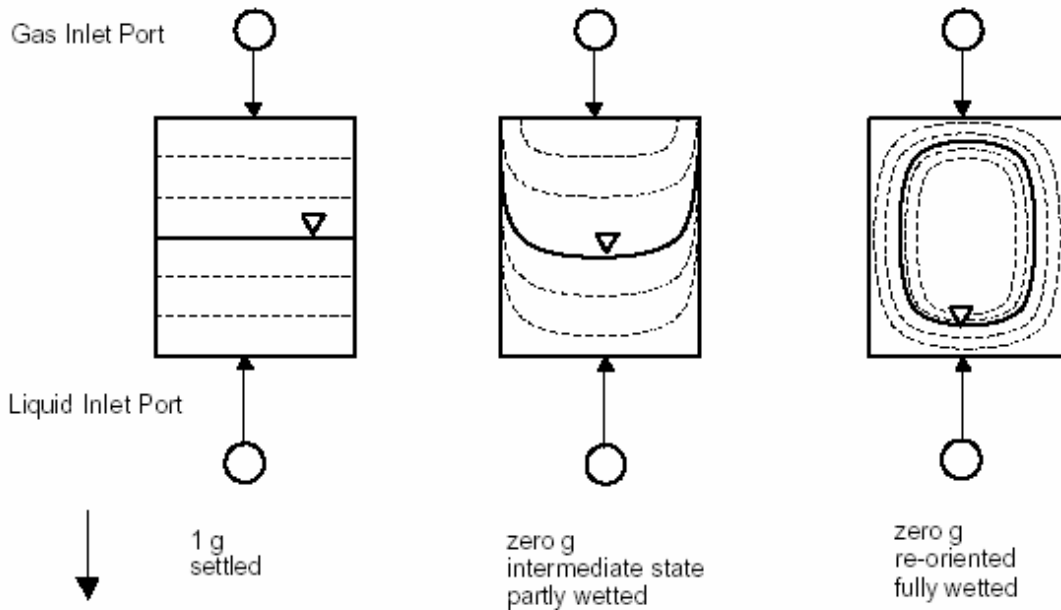
Fig. 25:   Fluid re-orientation schematic

This approach allows defining the required equations as add-on set in the CONTINUOUS block of the tank model with relations for the change of surfaces, contact areas, characteristic lengths, scaling factors and other selected parameters only.

All other basic relations for heat & mass transfer and thermodynamics are still valid.

Fluid Sloshing

The fluid sloshing might be caused by one or more sudden changes of the effective gravity orientation and/or level.

The effective gravity changes induce inertial forces on the liquid to be balanced with pressure and friction forces. In case the liquid can give way because of topological conditions, the liquid might be accelerated relative to the tank wall and start to slosh.

This movement is attenuated by friction forces in the liquid and at the liquid/wall interface, and by pressure and friction forces exerted by the ullage gas to the liquid free surface.

The sloshing can lead to very complex fluid movements depending on the existing disturbances. If the disturbances level off, the sloshing is damped by frictional effects, and finally the fluid is coming to the reoriented or settled state depending on the final effective gravity level and orientation.

For COMPTAS the modelling of sloshing may be extend towards the representation of the sloshing mode under the following convention:
- sloshing starts from settled or re-oriented conditions with an effective gravity (level/orientation) step change as excitation
- the first liquid/gas nodes are always in contact with the liquid/gas inlet ports
- the last liquid/gas nodes are always in contact with each other
- the sloshing motion will be represented by a damped linear oscillation of the bulk liquid mass
- the fluid surfaces (liquid and gas) are assumed to stay plane and normal to the sloshing radius vector
- the characteristic time, damping factors, etc. are obtained from the linearized theory
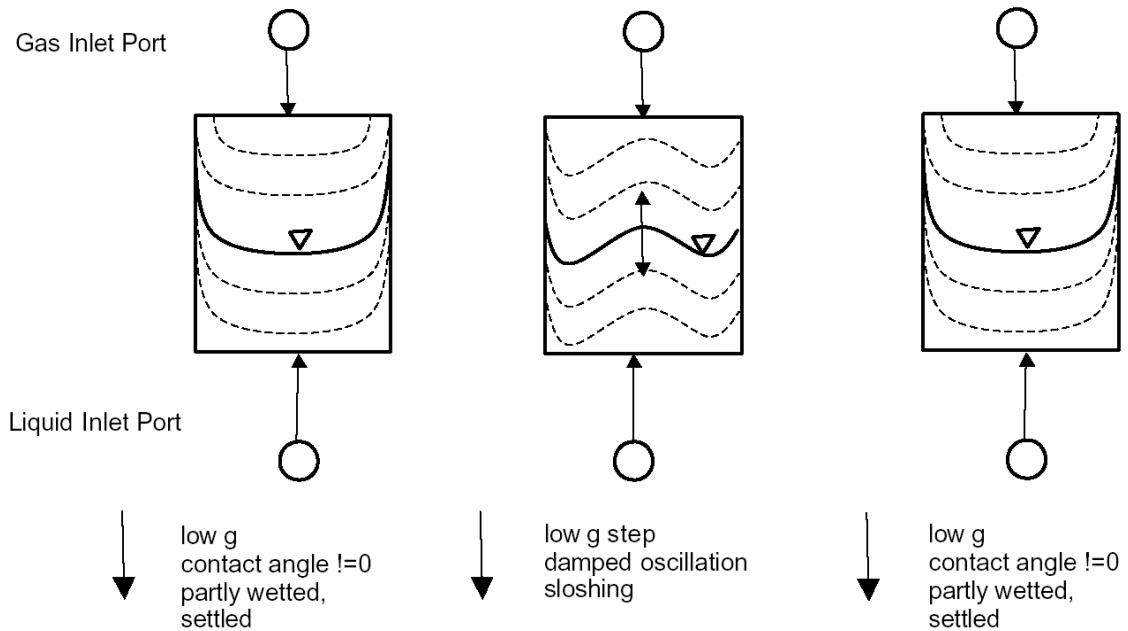
Fig. 26:   Lateral fluid sloshing from re-oriented state with change of effective gravity level

Validation

The validation of modelling/performance requirements can be achieved by verifying the analytical performance of COMPTAS for certain reference analysis cases and comparing the results with certain reference test cases. Presently this kind of validation has not been carried out in the frame of the COMPERE project. One reference case could be the AIR LIQUIDE test case01 (AL_TC1) with LH2 pressurized with HeG, for thermal stratification at earth gravity with boil-off losses through the gas inlet port.

Another reference case could be the AIR LIQUIDE test case02 (AL_TC2) planned for the LN2 cryostat for fast depressurization and sloshing. Currently, no cryogenic fluid properties are implemented in COMPTAS. Therefore both reference cases can not yet be analyzed.

However, in order to demonstrate the ability of COMPTAS to analyze such problems, the test case AL_TC1 can be analyzed as test case AS_TC1a for N2O4 as liquid propellant, N2 as pressurant, room temperature and a supply pressure of 1 bar. A comparison with test data and the validation of the COMPTAS performance for thermal stratification is presently not possible due to lack of test data for this pseudo reference case.

Conclusion

The COMPERE engineering S/W for the propellant tank analysis COMPTAS_01 (beta version) has been developed within the EcosimPro simulation environment for WINDOWS-NT on a PC. The S/W is operable for storable propellants in a cylindrical tank with insulation and fluid filling / depletion / pressurization processes.

A validation of the S/W performance is pending due to lack of appropriate test data. Currently, no cryogenic fluids or other than cylindrical tank shapes can be handled. Also no effects like sloshing, re-orientation, geysering and spin can be analyzed. However, these topics can be implemented in the future as outlined above.

5.4 Three-dimensional liquid sloshing in a cylindrical container in case of lateral acceleration and large Bond numbers

Experiments have been carried out to examine the sloshing behaviour of water in a cylindrical container. The test setup is plotted in the following picture.
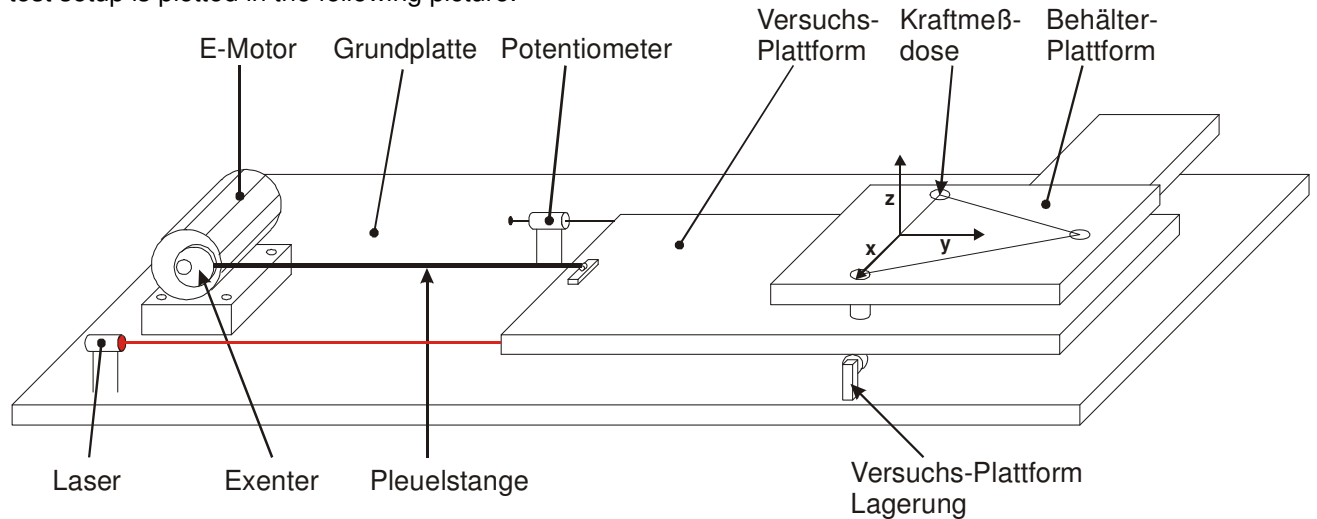

Fig. 27: Experimental setup

The test tank has been mounted on a force measurement platform. This way the sloshing forces can be measured. These are then compared to equivalent numerical results.

Force data are of general interest for any upper stages development since sloshing forces have to be controlled within a defined frame. If sloshing forces become too high, then the stage may get out of control. Especially in case of closed loop simulations (coupling of the sloshing behaviour with the stage's control mechanism) the sloshing forces have to be very accurate. Any additional numerical disturbance will lead to errors in the coupled analysis. The present test case and the numerical assessment are therefore a first important step in order to verify the accuracy of the numerically obtained sloshing force profiles.

The cylindrical tank has a radius of R = 8.5 cm and is subjected to a periodic forcing (maximum amplitude 3 mm). The working fluid is water. The following picture shows the liquid sloshing inside the cylindrical container.
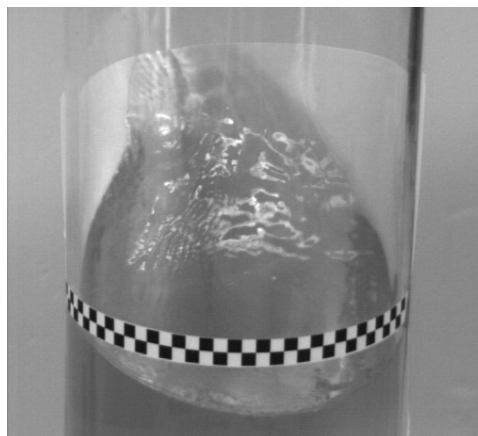

Fig. 28: Maximum deviation of sloshing liquid (2.3 Hz, liquid is rotating)

The experimental results have been compared to numerical results obtained with the Flow-3D software. The results show that the forces on the container wall increase rapidly when the resonance frequency (here 2.4 Hz) is approached. If the frequency of the tank is increased beyond 2.25 Hz, then a swirling wave motion will occur.

There is a very good agreement between the experimental results and the numerical simulations. However, the simulations give less swirling (see following pictures).
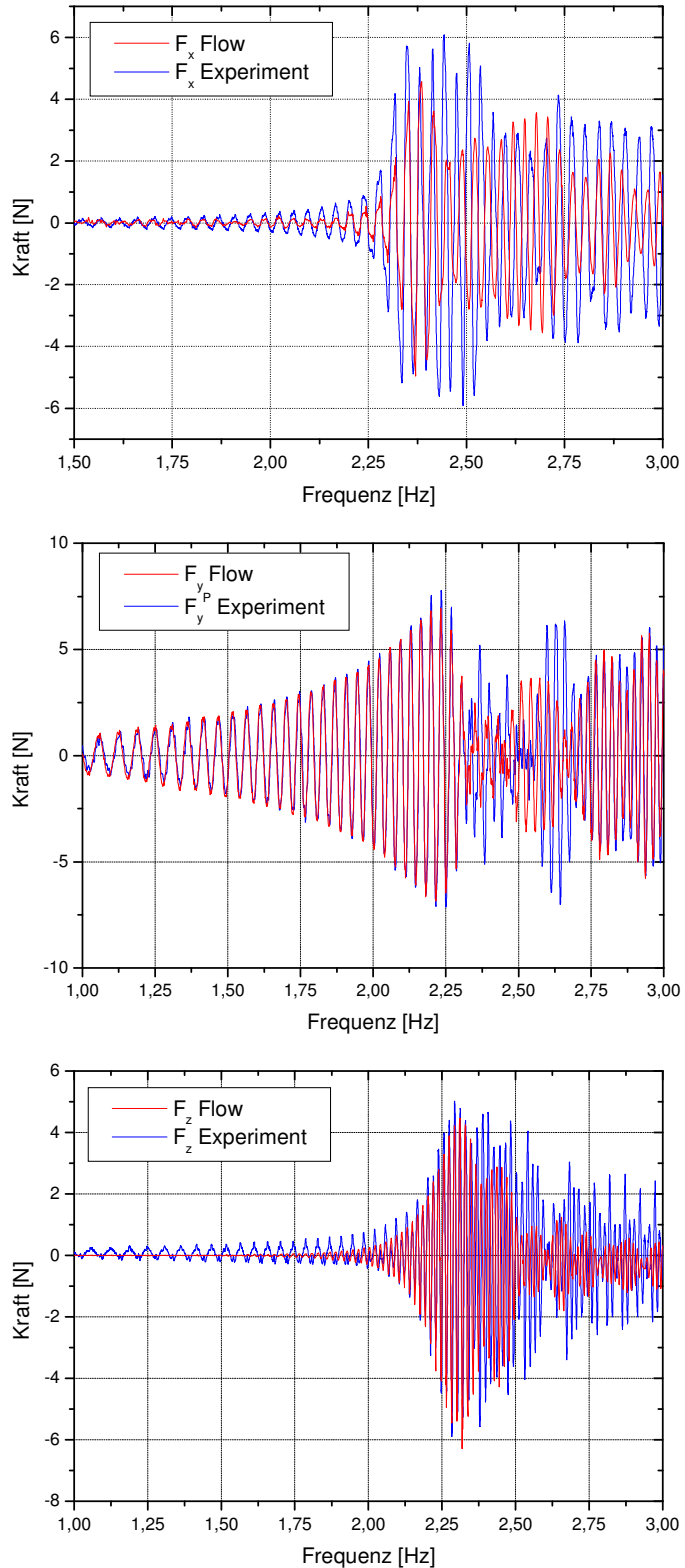

Fig. 29: Comparison of experimentally and numerically obtained sloshing forces for the three directions

5.5 Modelling of bubbles and drop formation and their motion for different acceleration levels

Bubbles may occur in upper stage tanks due to different reasons:
- Boiling due to the heat flux into tank (for instance in case of Ariane 5 ESC-B) where the ebullition point liquid/gas is for instance near to 20-22K for LH2 inside tank and 80-85K for LOX inside tank), which becomes most critical during low gravity phases due to the lack of convection.
- Bubble entrapment during the sloshing motion.
- Temperature conditioning process performed prior to engine restart. In this case pressure decreases in order to cool the liquid in the tank. As pressure decreases below the saturation pressure, bubbles are created.

The performed work was subdivided into:
- Literature survey with respect to bubbles and drops, their formation, detachment from the wall and their motion (depending e.g. on the gravity field or the bubble size)
- Based on the available literature theoretical model development for isothermal problems
- Formulation of dimensionless numbers (Fr, We, Re...). A similarity with respect to different bubble sizes or material parameters was obtained.
- Modelisation of the fundamental equations to model the behaviour of bubbles and drops solved either analytically or numerically by FORTRAN and Matlab
- Comparison with solutions obtained with commercial CFD tools such as FLOW-3D.

The overview below depicts a logic concerning the relevant dimensionless numbers. The matrix enables the determination of the bubble shape as a function of the defined dimensionless parameter.
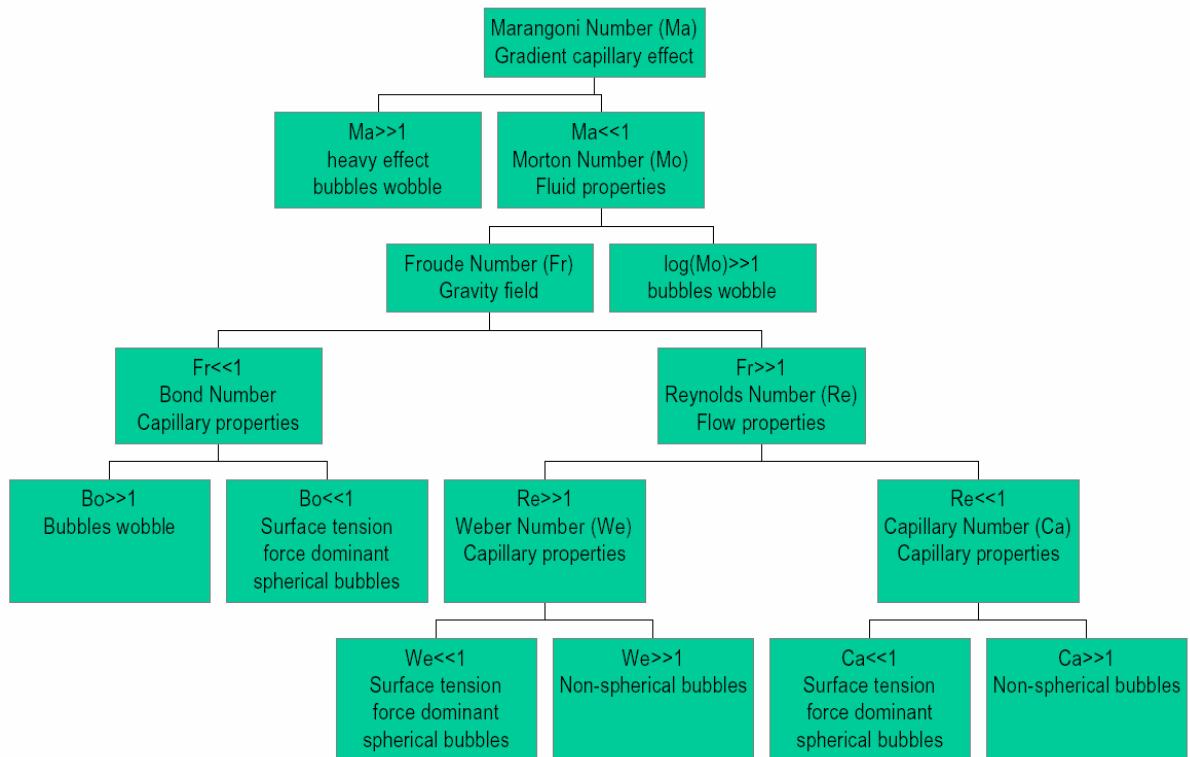

Fig. 30:   Overview on a matrix to determine the bubble shape

COMPERE

Dok.Nr./No.:	TE51-RIBRE-TN-0067
Ausgabe/Issue: 1	**Datum**/Date: 15.06.07
Seite/Page: 36	**von**/of: 67

Comparison of bubble formation theory with Flow-3D

Flow-3D is a commercial software CFD code used at Astrium GmbH in a variety of space applications to analyze behaviour in tanks and propulsion systems. It uses the numerical solution algorithms to approximate the Navier-Stokes equations.

In a first step isothermal single bubbles were investigated. A number of investigations exist. An example of a continuous bubble flow forming at a horizontal surface in a 1g environment is shown in Fig. 31.
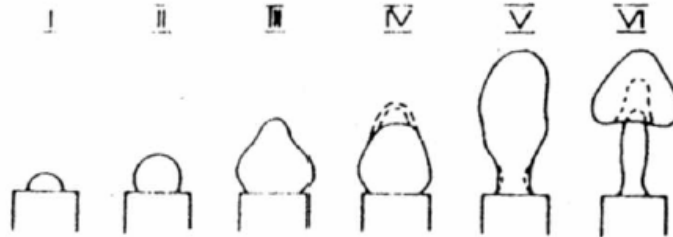
Fig. 31: Bubble formation according to Räbiger and Vogelpohl's Model

Within the calculation of bubbles and free surface flows, gas is treated as a region of uniform pressure and temperature. The bubbles are thus treated as single node regions. The numerical problem can then be drastically simplied. The regions occupied by the fluid are identified as regions where the fluid fraction function is non zero. A view of the equivalent bubble flow, as shown in Fig. 31, is given for the FLOW-3D calculation in Fig. 32.
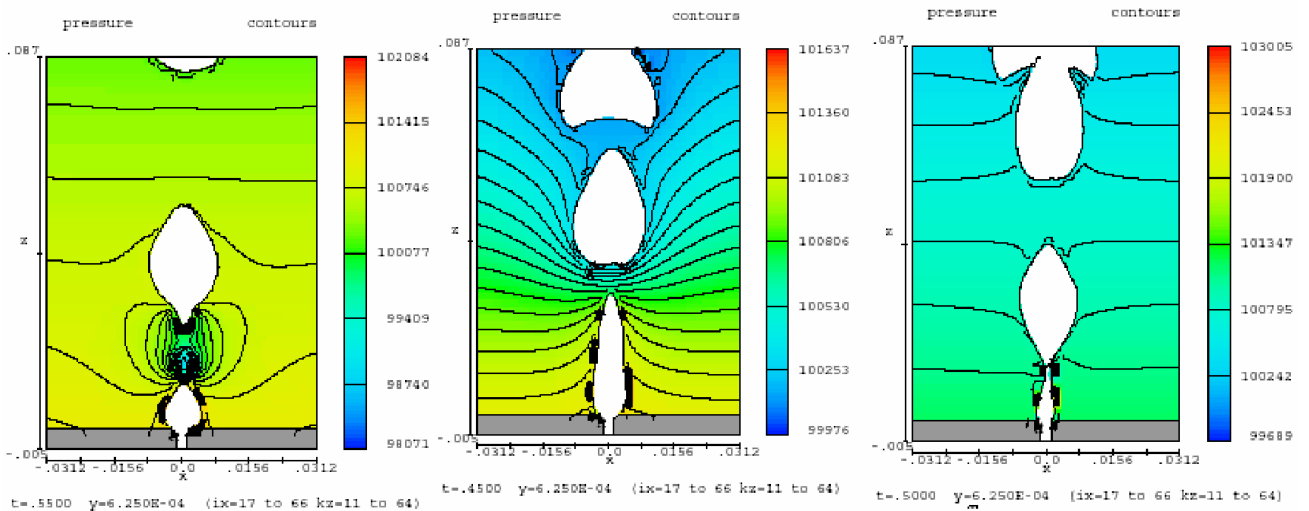

Fig. 32: Results of Flow-3D bubble modelling (good correlation with respect to theory)

It becomes evident that the behaviour of the bubbles is very similar to the one shown in Fig. 31. Same as in Fig. 31 the second bubble penetrates the first one during it's rise as a consequence of the velocity field behind the bubble (compare right pictures in Fig. 31 and Fig. 32).

The evaluation of the pressure and temperature of void regions depends on the void region model. In Flow-3D there are five different ways to model a void region:
- Fixed Pressure Regions, when densities of the fluid and the gas differ significantly, then the small variation of pressure within the gas and the gas inertia can be neglected.
- Cavitation Regions, regions open up in the fluid when the local drops below a critical value called cavitation pressure. The new region is treated as a bubble with a fixed pressure equal to the cavitation pressure.
- Adiabatic Bubbles, when a volume of gas gets trapped in a confined region, the gas pressure can not stay constant. FLOW-3D uses an incompressible one fluid mode, with the approximation of perfect gas.

- Conservation Void Regions
- Homogeneous Bubbles. In this case the void regions are only described by the local fluid fraction in the cell. A fluid fraction of zero corresponds to a cell where only gas is present. A value of one states that there is only liquid.

As a result of the performed analyses it became clear that the FLOW-3D software is able to model the bubble motion inside a liquid with good accuracy. It should be noted that the bubbles have to be resolved by a sufficient number of cells in order to have a good solution. Generally bubbles should not be resolved with less than 10 cells.

5.6 Depressurization Analysis of LN2 under 1g Conditions

5.6.1 Experimental Depressurization Analysis of LN2 under 1g Conditions

Goal of the present analysis is to investigate the behaviour of liquid nitrogen in case of a fast depressurization of the tank. Thus a glass dewar has been selected which stores the liquid nitrogen at a selected pressure inside a vacuum chamber (see Fig. 33). The dewar is connected to the vacuum chamber by a valve which can be opened instantaneously. Thus a pressure relief will occur inside the dewar. Due to the pressure loss the liquid nitrogen will overheat and boiling will occur.

Fig. 33:   Glass test vessel inside vacuum chamber. The test chamber is covered with MLI in order to reduce radiative heat, especially from the light source.

Test Setup

The test setup principally consists of a sealed glass test vessel, which is located inside a vacuum chamber. The test vessel and the vacuum chamber are connected via an outflow pipe, which is lockable by an electromagnetic valve. The principal test setup with the glass dewar (test vessel) inside the vacuum chamber can be seen in Fig. 33. A schematic sketch of the experimental setup is shown in Fig. 34 illustrating the instrumentation of the experimental setup including the different valves for the nitrogen supply (valve No.1 and No. 2), the evacuation (valve No. 4) and venting (valve No. 5) of the vacuum chamber and for the depressurization of the test vessel (valve No. 3). Pressure sensors are used to measure the pressure inside the vacuum chamber and inside the test vessel.

Temperature sensors are located at different positions inside and outside the test vessel and inside the vacuum chamber. The test vessel made of glass is sealed with a stainless steel cover, which has a lead through for the filling pipe and the outlet pipe, which serves for venting as well as for the lead through of the temperature sensors.

In addition to the data recording of the temperature and pressure sensors a video system was used to observe the boiling process. For illumination of the vacuum chamber a halogen light was mounted inside the vacuum chamber (see Fig. 33). The test case experiment the test vessel was laterally wrapped with sandwich insulation foil (Mylar, aluminum coated polyester foils) to minimize local heating of the test vessel due to direct heat radiation from the halogen light. A sketch of the test setup is shown in Fig. 34.
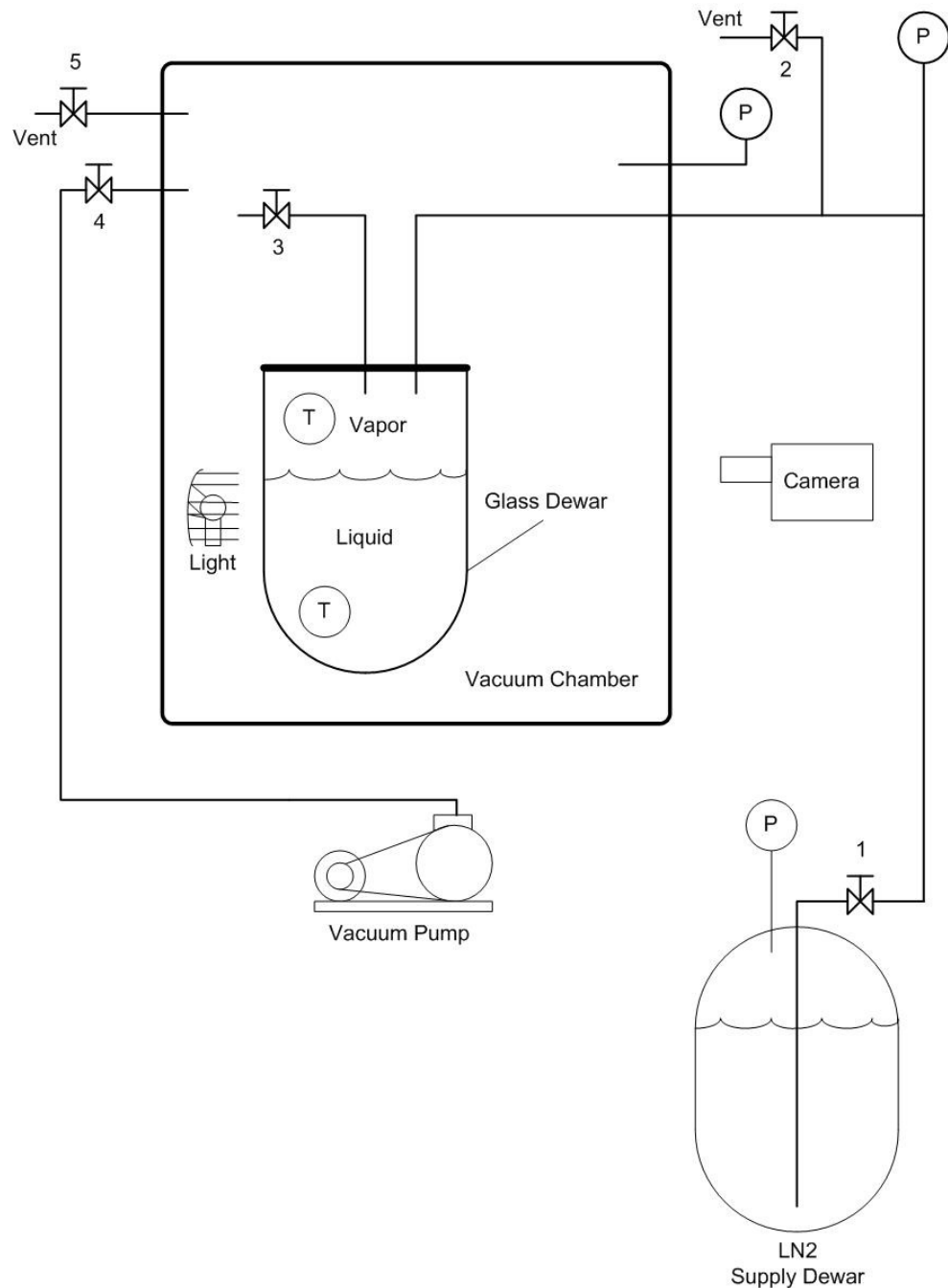
Fig. 34:   Sketch of the depressurization test setup

Results of Test 3a

This test case was selected proposed as a benchmark test within the Compere project. This test is the start of the test campaign No. 3 and No. 4 (same date) after filling of the test vessel under ambient pressure (1bar) and the following pressurization up to the initial pressure.

The following graphs show the pressure and the temperature evolution in the tank.
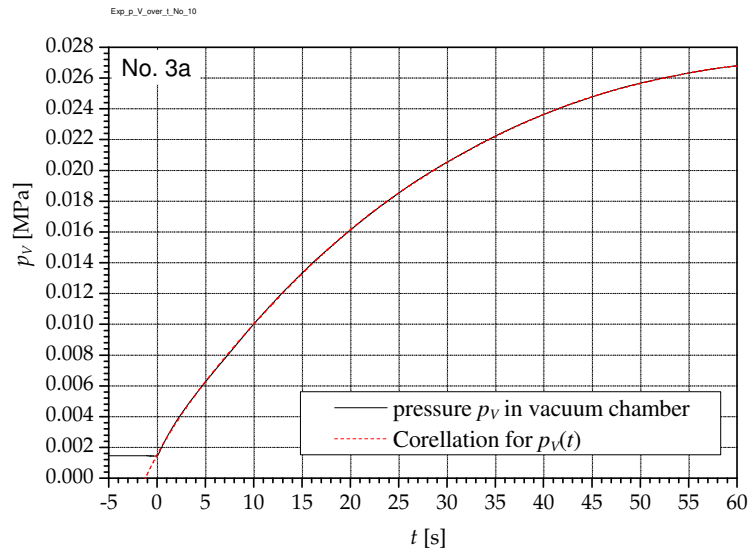
Pressure histories (No. 3a):

Fig. 35:   Pressure evolution $p_V(t)$ in the vacuum chamber during the depressurisation (No. 3a)
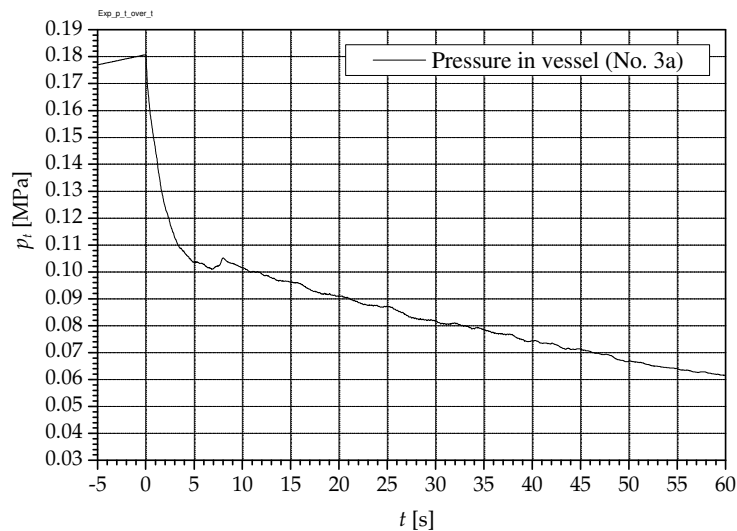
Fig. 36:   Pressure evolution $p_t(t)$ in the vacuum chamber during the depressurization (No. 3a)

Temperature histories (No. 3a):
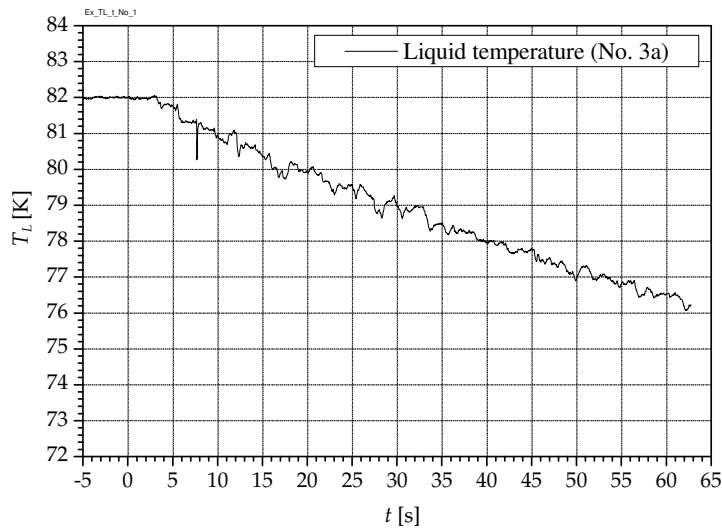
Fig. 37: Evolution of the liquid temperature $T_L(t)$ during the depressurization (No. 3a)
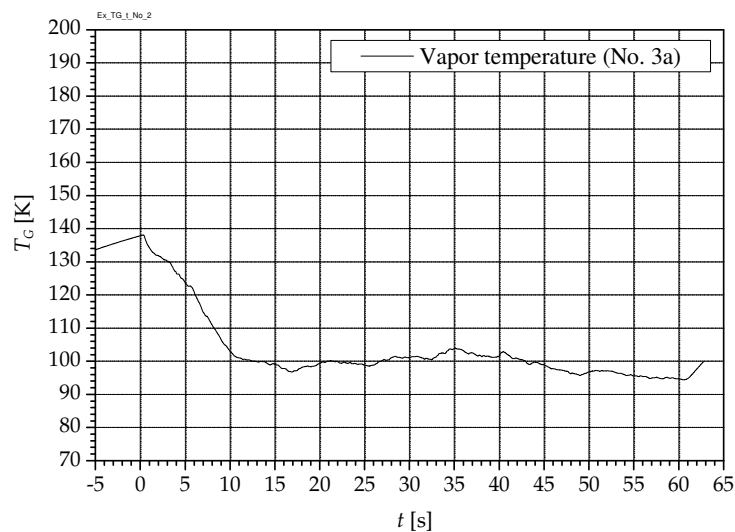
Fig. 38: Evolution of the ullage temperature $T_G(t)$ during the depressurization (No. 3a)

The experiments show the following behavior:
- The liquid fill level changed from test to test due to the amount of liquid which has been evaporated.
- Total number of nucleation sites decreased when depressurization is repeated. Lower fill levels seem to lead to lower number of nucleation sites at the temperature sensor.
- Boiling retardation (later activation of nucleation sites)
  - From test to test a trend to boiling retardation was observable (later occurrence of large bubble formation).
  - The number of active nucleation sites seems to vary
  - Apparently the history of the depressurization processes seems to have an influence. It is therefore of importance to include information e.g. concerning the time the liquid has been stored in the reservoir and the different processes which have been performed before the experiment was started.

Fig. 39 shows S-VHS Video images of the test number 3a.

Fig. 39 :   Test No. 3a: Start and end of experiment, images for $t = 0$ and $t = 60\,\text{s}$

The following figures show freeze images from the recorded video of the test case. Some specific points of time are depicted in detail (e.g. formation of a large vapour bubble at the vessel bottom starting at $t = 7.28\,\text{s}$).

There are no permanent nucleation sites at the vessel wall. During the experiment large bubbles are formed two times at the bottom of the test vessel. The figures below depict the high speed images of the liquid temperature sensor.
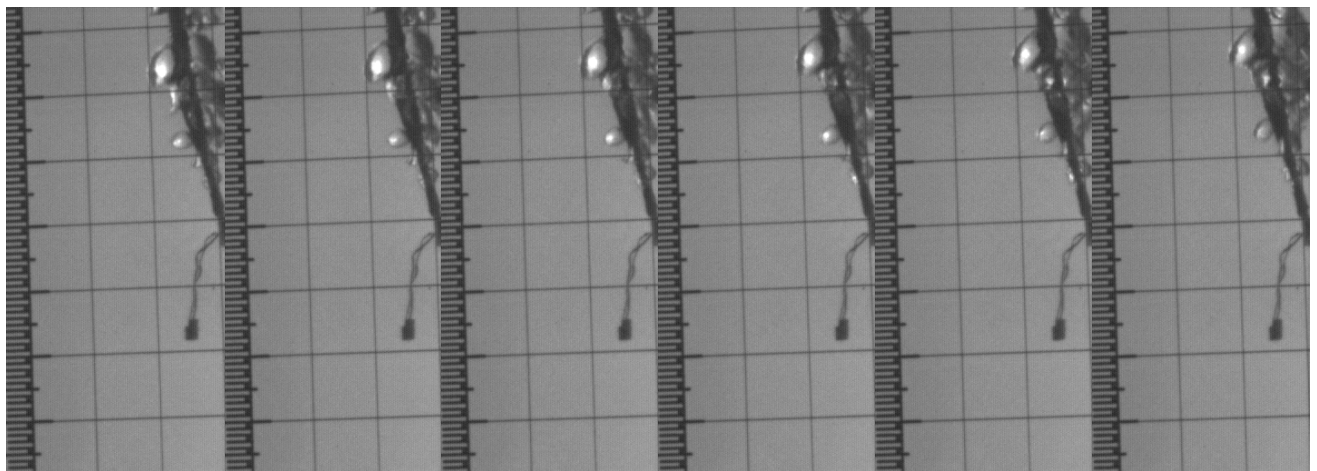
Fig. 40:   Test case 3a: No. 2518 - 2523 (size 41 %, bright: 68%, contrast 70 %), 500 Hz

Conclusion

The depressurization experiments consist of a glass Dewar which contains liquid nitrogen. The dewar was stored in a vacuum chamber. Using a valve the Dewar was connected to the vacuum chamber. Evaporation occurred when the valve was opened and the liquid becomes overheated. A single temperature sensor, being submerged in the liquid, turned out to be the main source of boiling being a well defined location in the tank. This allowed the numerical modelisation of the process. Consequently the experiment was chosen as the basis for benchmark experiments for numerical analyses. The analyses imply clear initial and boundary conditions as far as possible. Thus they can be considered a suitable basis with respect to first comparisons with numerical analyses.

5.6.2 Numerical Depressurization Analysis of LN2 under 1g Conditions

This chapter discusses analyses carried out to investigate the capability of the CFD software FLUENT and FLOW-3D to simulate the boiling of cryogenic liquids subjected to a fast depressurisation process. Such de-pressurization processes may occur during missions of cryogenic upper stages to change the liquid conditions and also to maintain the pressure in the technical allowed range. Due to the pressure decay the liquid will overheat. Thus evaporation at the free surface and local boiling will occur. Goal of the present analysis is to find an adequate way of modelling the depressurization process with available software tools (FLOW-3D/FLUENT).

FLUENT's Mixture model

The mixture model was selected in FLUENT to simulate the depressurisation behaviour. Main aspects of this model are:

- Interpenetration of phases. The volume fractions of gas and liquid can vary between 0 and 1.

- Phases can move with different velocities (slip velocities).

The continuity equation for the mixture, the momentum equation for the mixture, the energy equation for the mixture, the volume fraction of the mixture and the algebraic expressions for relative velocities are solved by the mixture model. In the used mixture multiphase model with slip velocity the drag function is estimated by using the Schiller-Naumann approach in FLUENT. In the used mixture model the phases are modelled as interpenetrating (i.e. no surface tracking and therefore no discrete bubble resolution). The slip functions are estimated according to Manninen et al. ref. [12].

Volume zones

The FLUENT model is subdivided into five volumes to enable different vaporisation rates with respect to the probability of evaporation in the different zones.

These zones are (compare Fig. 41):

- Pipe Volume,

- Upper Volume,

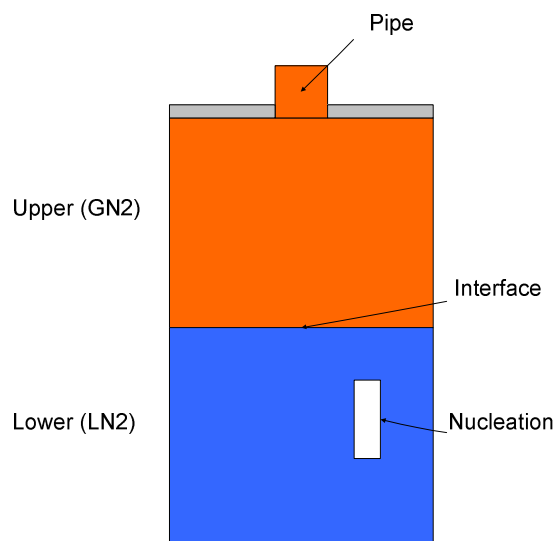- Interface Volume,

- Nucleation Volume,

- Lower Volume.

Fig. 41: Volume zones in FLUENT model

The pipe volume is used to model the outflow pipe conditions. The upper volume represents the gaseous volume within the test vessel. The interface volume represents the boundary layer between the upper and the lower volume. The nucleation volume represents the volume with the highest vaporisation rates during the tests in the vicinity of the temperature sensor T_L. The lower volume represents the liquid phase in the test vessel. A schematic of the test vessel volumes is shown in Fig. 41.

For simplicity the spherical bottom part has been replaced by a flat bottom. The initial liquid volume is however the same as in the experiment. No influence on the validity of the results is therefore expected.

Model limitations

The applied mixture model approach imposes a number of limitations. These are:
- Gas bubble generation is performed for each zone parameter by setting a minimum gas fraction and a maximum gas fraction. In this corridor evaporation / condensation occurs. Thus phase change only occurs where a certain fraction of gas is already present.
- In all five zones of the FLUENT model evaporation and condensation can occur.
- Detachment of gas bubbles from tank walls is neglected.
- Heat fluxes from wall to the fluid are in all zones zero.
- Nucleation only occurs in cells where a certain minimum gas volume fraction is present (here 1% of gas), e.g. in cells where a solid wall is present. This way active nucleation sites can be preset.
- Vapour bubbles are not depicted separately. The amount of gas volume in a cell corresponds to the volume fraction in the mixture model.
- No surface tension effects can be modelled. Thus the model only allows cases with high Bo-number.
- The velocity of the vapour leaving the test chamber is sonic throughout the simulation. Thus there is no influence of the pressure in the vacuum chamber on the results. This coincides with the observation in the experiment. The vacuum chamber is therefore neglected in the numerical simulation.

In addition the FLUENT model assumes for the outflow:
- The potential energy differences between inlet and outlet are neglected.
- An adiabatic reversible process is considered.
- Heat transfer to the test vessel is neglected.
- Presently only a single gas phase can be modelled.

Initial and Boundary Conditions

The initial and boundary conditions for the simulation are given in Table 4.

Initially all liquids are assumed to be at rest ($V_x = V_y = V_z = 0 \frac{m}{s}$).

	Temperature [K]	Pressure [Pa]	Fluid Fraction [%]	Gas Fraction [%]
Gas Phase (GN_2)	137.9	180750	0.001	99.99
Interface	82	180750	97	3
Liquid Phase (LN_2)	82	180750	99.99	0.001
Nucleation	82	180750	95	5
Cover Plate	215.4	180750	--	--
Outflow Pipe	137.9	25000	0.001	99.99

Table 4: Initial and boundary conditions of the FLUENT model

Concerning the location of the different parts in the vessel see the sketch view in Fig. 41.

The results of the numerical analysis compared to the experimental results are shown in the following graphs.
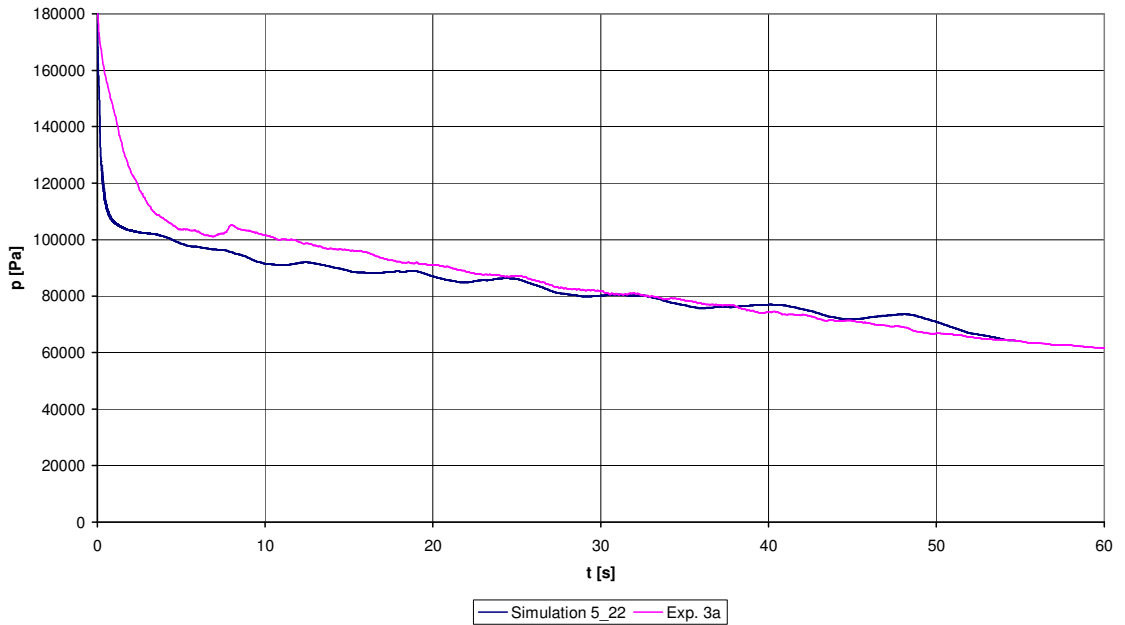
Tank pressure:

Fig. 42:   Pressure history in tank of simulation 5_22 (experimental results vs. numerical approximation)
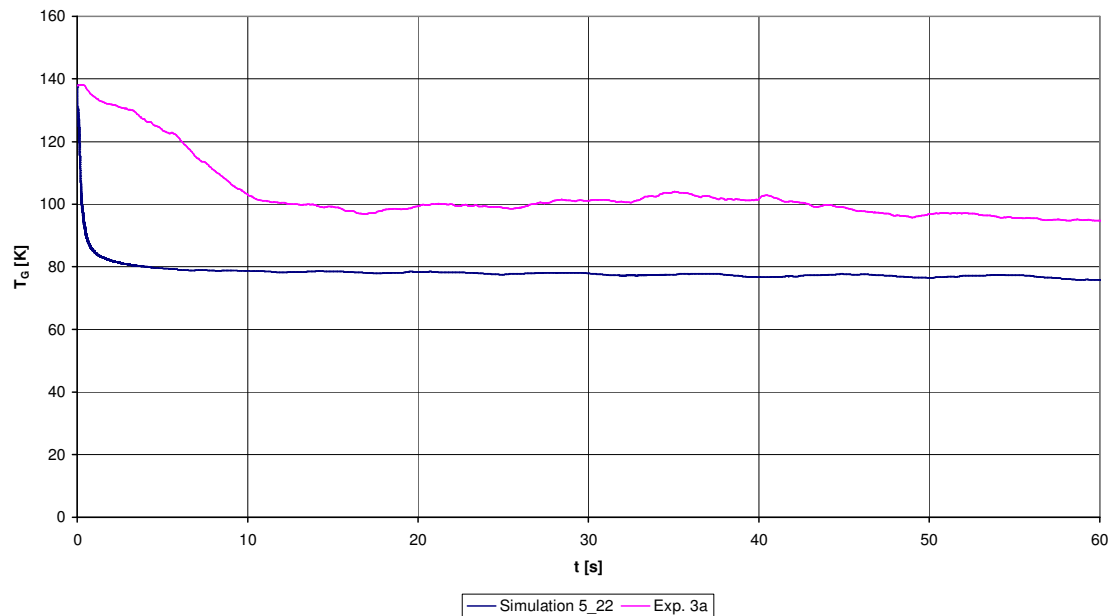
Gas temperature:

Fig. 43:   Gas temperature history in tank of simulation 5_22 (experimental results vs. numerical approximation)
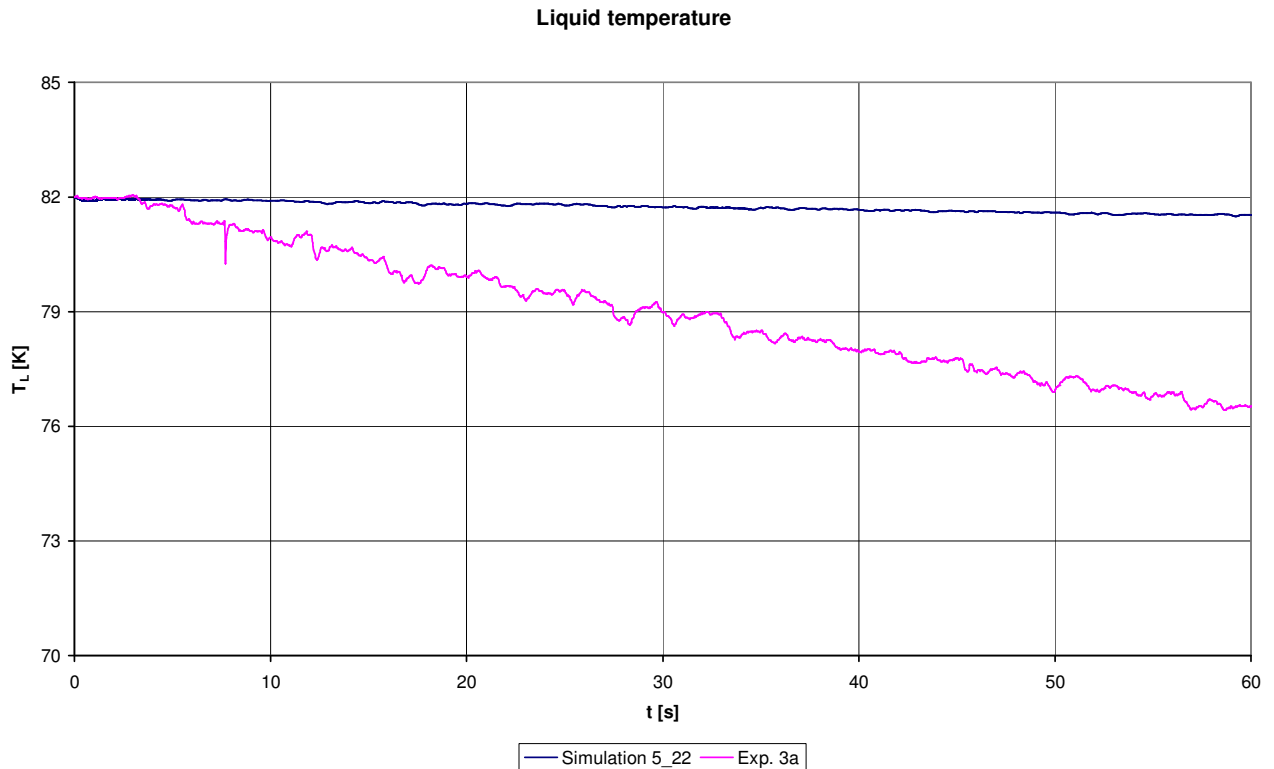
Liquid temperature:

Fig. 44: Liquid temperature history in tank of simulation 5_22 (experimental results vs. numerical approximation)

Result: Applying the proposed model it seems to be possible to investigate this kind of depressurization under high gravity conditions. All relevant physical models are available. Generally the initial pressure loss is too high while the more steady part of the pressure history is similar. Deviations with respect to ullage and liquid temperatures are very much linked to these initial differences. The reasons for these differences are still not completely understood. On the one hand the orifice diameter has been fitted with respect to the pressure gradient at t = 0 using nitrogen gas under ambient temperatures. It is however known that phase change including freezing may also occur inside the nozzle. A similar behavior occurs when depressurizing an upper stage tank. One possible solution is thus that the orifice diameter in the experiment has reduced during the depressurization process. Errors in the programming of the UDFs are also possible. However the strong initial pressure gradient was found for both FLUENT and FLOW-3D. As a consequence of this discrepancy more emphasis should be put on the accurate evaluation of the outflow mass flux under cryogenic conditions. In case of the sounding rocket experiment SOURCE, where a depressurization experiment under 0g conditions shall be carried out, the mass flux determination therefore includes additional pressure and temperature measurements. Still the results indicate that the proposed model is able to handle phase changes. Future applications are for example the evaluation of tank filling where strong boiling can be expected or the evaluation of boiling processes under high Bo-number conditions, e.g. when the stage is in a spin mode during its ballistic phase.

Flow-3D Model

Drift Flux for two Phase Flow

The drift model describes the relative flow of two intermixed fluid components, one continuous and the other dispersed, with different densities. The drift model is used in the situation described below which corresponds to the model used for the analysis:

Incompressible and compressible fluid mixtures:
In this case, the density of the compressible gas is defined by the equation of state, while the incompressible material has a constant density, which is always assumed to be much larger than the gas density. The gas properties are defined the same way as for any compressible fluid case.

There are two available drift-flux models - linear and quadratic, referring to the approximation of momentum coupling between the two phases. The drift coefficient in the linear model describes a Stokes-type, viscosity dominated flow of the continuous phase around particles of the dispersed phase. It is the reciprocal of the drag coefficient for the momentum exchange term, which is a function of the fluid viscosity and average particle size. The drift velocity in this case should not become too large; otherwise, the linear approximation may not be accurate.

The quadratic drift-flux model takes into account both viscous and pressure forces acting between the two phases, covering a wider range of flow types. It is the recommended model. Required input is the drag coefficient, the average particle size and the Richardson-Zaki coefficient (used for closely packed dispersed phases).

In addition the coalescence of the dispersed phase droplets into a continuous fluid at a defined volume fraction can be modelled in both linear and quadratic cases. This may be important in such devices as oil/water separators. A possible application may also be the modelisation of a phase change (boiling) situation in a pipe. In the present case the model has not been used since the gas volume fraction is still small.

Flow-3D results

Within this section the results obtained from the FLOW-3D two-phase model with incompressible liquid and compressible gas phase are presented.

The following figures show the history plots of the pressure, surface height, volume of fluid, fluid surface area, phase change rate and the phase change mass transfer rate, respectively. The analysis results are limited in the time domain to 9 seconds. However, this is the region of major interest because of the transient behaviour of the two-phase model.

pressure: history point 1

(pressure multiplied by 1.e-05)
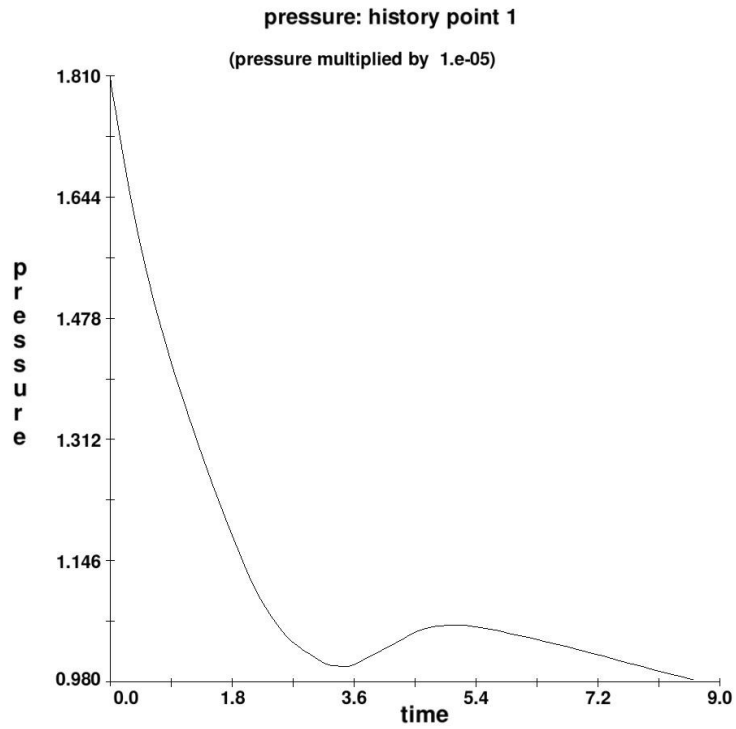
FLOW-3D
14:59:30 08/05/2005 iykc   hydr3d: version 9.0 win32-cvf 2005
Depressurization test LN2   1

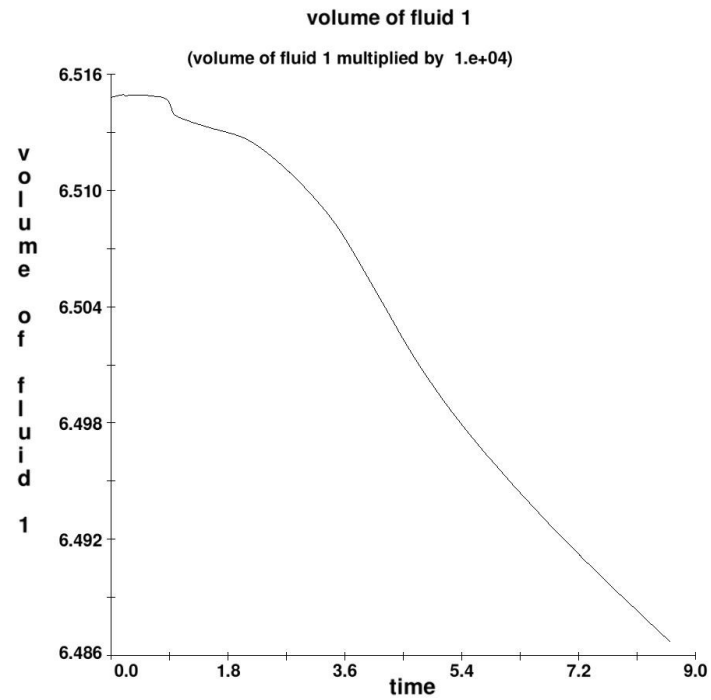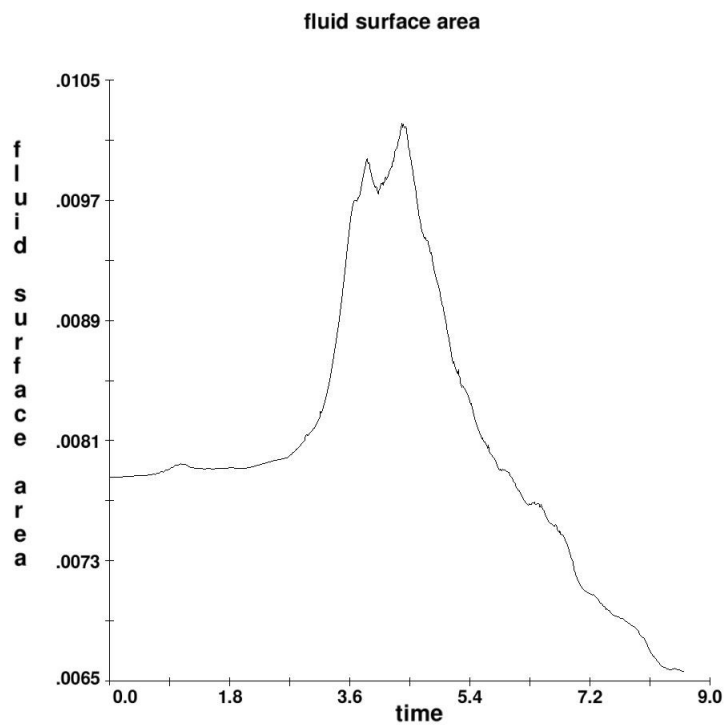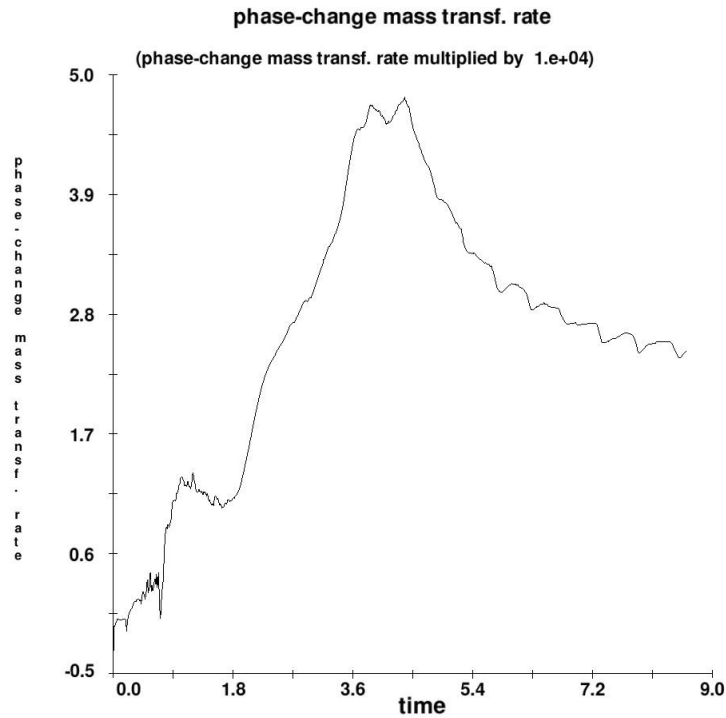Fig. 45:   Pressure history profile (FLOW-3D two-phase flow model) [Pa]

surface height: history point 1
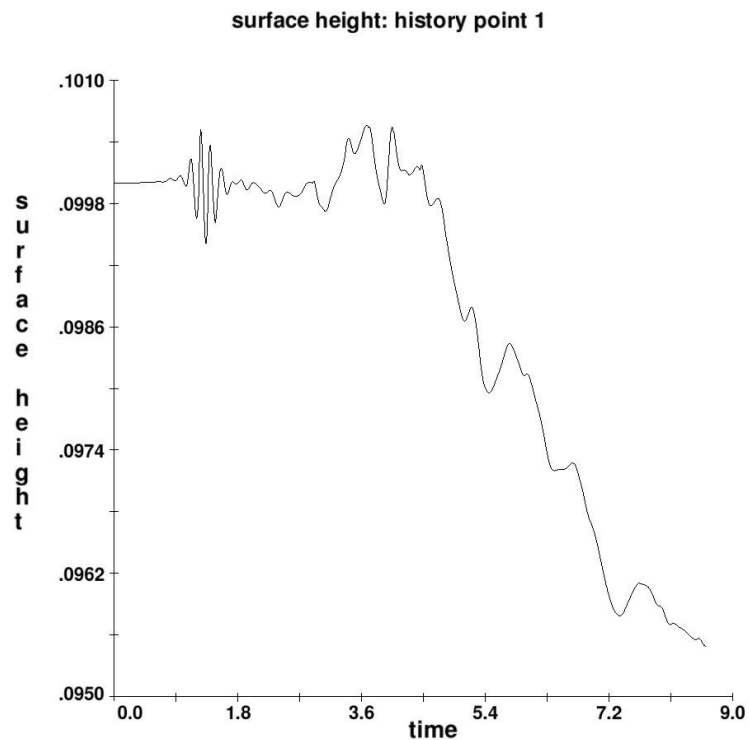
FLOW-3D
14:59:30 08/05/2005 iykc   hydr3d: version 9.0 win32-cvf 2005
Depressurization test LN2   2

Fig. 46:   Surface height history plot (FLOW-3D two-phase flow model) [m]

volume of fluid 1

(volume of fluid 1 multiplied by 1.e+04)

Fig. 47:   Volume of fluid history plot (FLOW-3D two-phase flow model) [-]

fluid surface area

FLOW-3D
14:59:30 08/05/2005 iykc   hydr3d: version 9.0 win32-cvf 2005
Depressurization test LN2   4

Fig. 48:   Fluid surface area history plot (FLOW-3D two-phase flow model) [m²]

Fig. 49:   Phase-change mass transfer rate history plot (FLOW-3D two-phase flow model) [kg/s]

The following pictures show the evaporation behaviour during the depressurization process (see Fig. 50).

It can be seen that evaporation occurs at the nucleation site, comparable to the experiment. However after a while the whole liquid area generates bubbles. This is expected to be a consequence of the numerical model. Bubbles are only generated in cells which contain a non-zero amount of gas. If bubbles do not rise fast enough then the neighbouring cells in the liquid will a minimum non-zero amount of gas after a certain time. This initial amount of gas is sufficient to initiate phase change in the cell. This way the bubbles will distribute from cell to cell.

It is expected that the predefined bubble diameter for gas bubbles in a cell, which is reasonable enough at the heater element, is however unrealistic in the liquid. Here only evaporation at the free surface should occur. Thus, if the model of rising bubbles is used, then the diameter should be sufficiently small in order to hinder propagation of gas bubbles into the liquid. Considering this aspect the FLUENT modelisation is expected to be more flexible compared to the presently available FLOW-3D model.
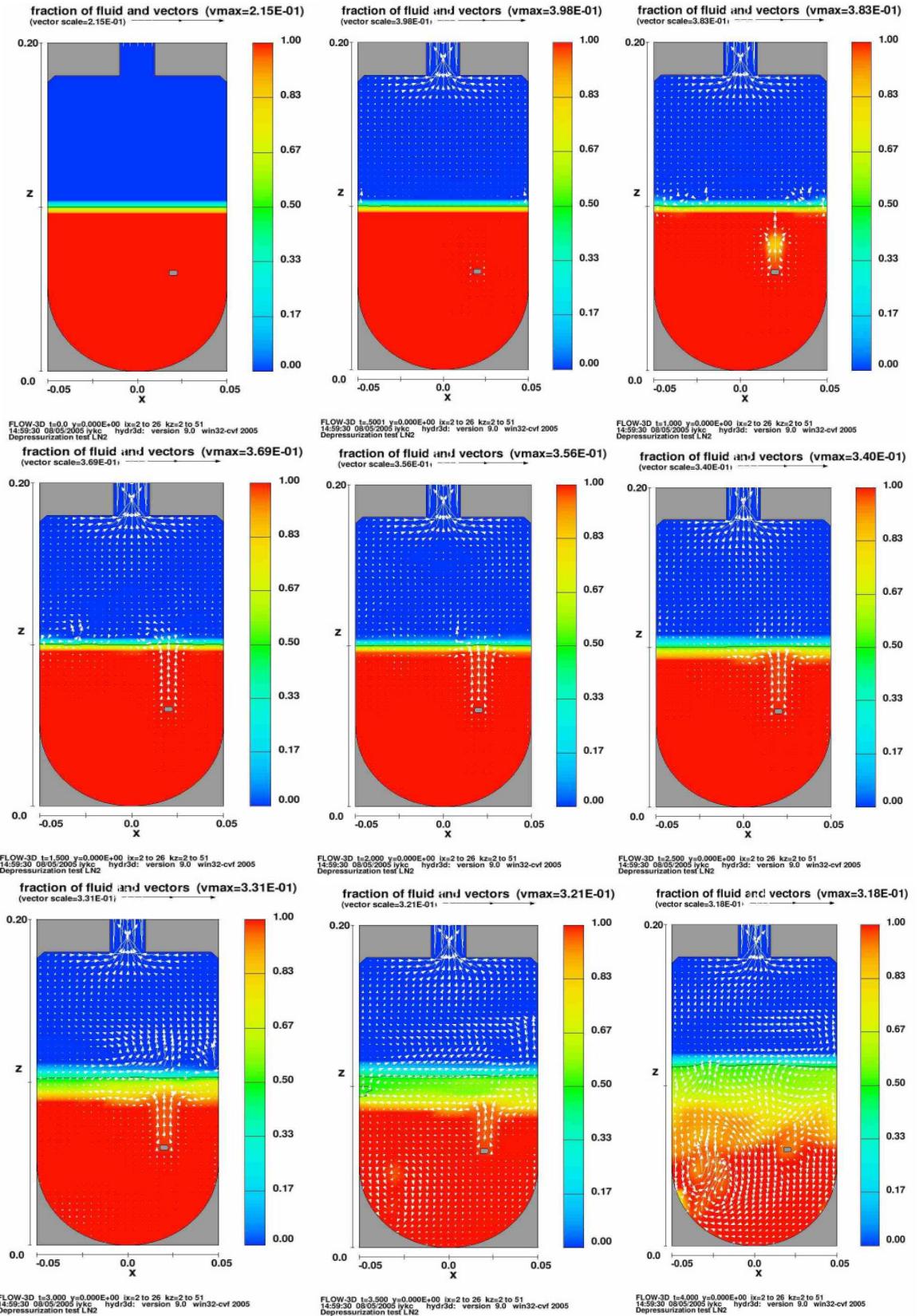
Fig. 50:   Evaporation behaviour during the depressurization process

Comparison of FLUENT and Flow-3D Results

To get an assessment of the performance capability of both models the analysis results of the FLUENT mathematical model and the results of the FLOW-3D model are compared with the test results of test 3a.

As can be seen in the following pictures the results obtained with FLOW-3D have a higher correspondence with the test results in the pressure time history as well as in the gas temperature time history as the FLUENT results. FLOW-3D shows, compared to FLUENT, during the first eight seconds a very high correlation with the pressure decrease measured during the test. FLUENT has a spontaneous drop in pressure at the very beginning. Thereafter, the profile fits more and more the measured pressure profile. The FLOW-3D pressure history has been terminated since the whole liquid has started to boil in contradiction to the experimental observation. This has already been explained above. Unlike to FLUENT and the experiment the initial gas temperature in the FLOW-3D analysis is set to 180° K instead of 140° K. However the FLOW-3D result shows a smoother decrease of the gas temperature than the FLUENT result. Since the orifice diameter is the same in both cases the FLUENT model should be checked with respect to programming inconsistencies.

Knowing that a final parameter adaptation for both models will lead to a reasonable increase of correspondence particularly in the transient phase at beginning of the investigation (first 10s) a second model evaluation has to be done for both FLUENT and FLOW-3D.
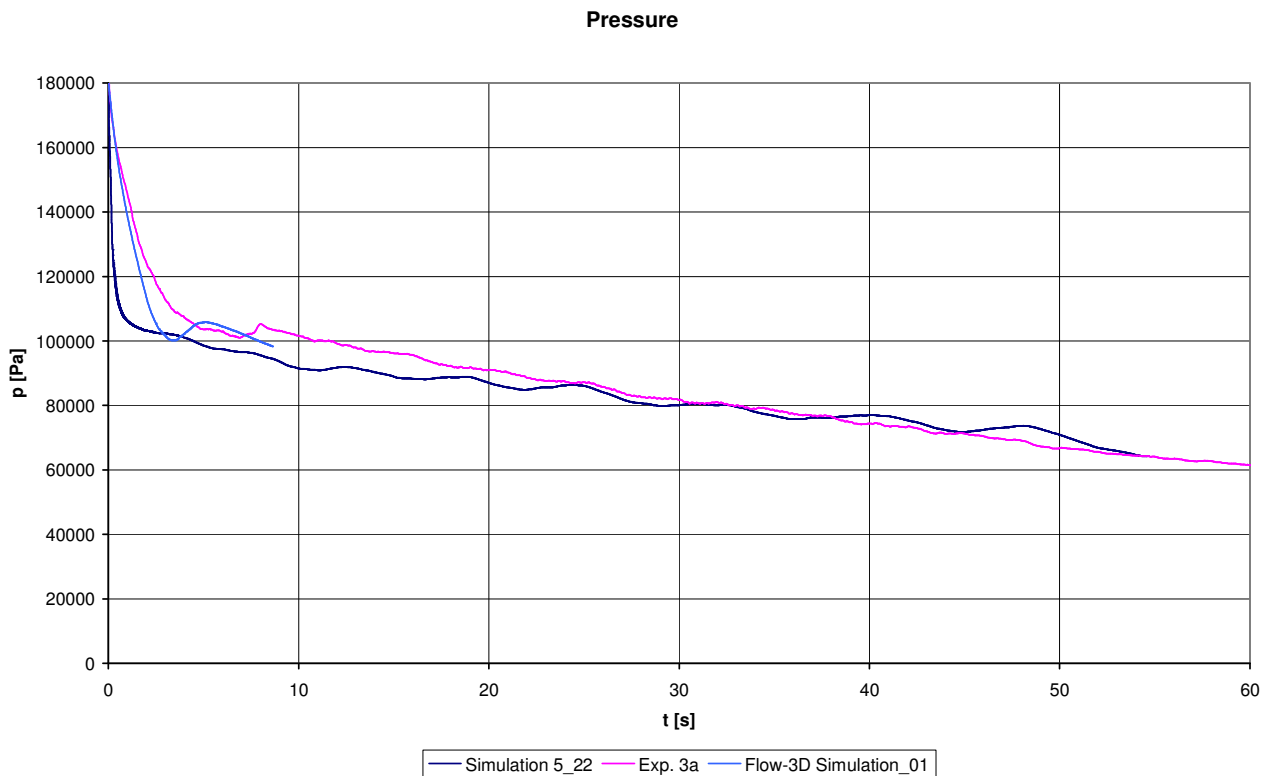

Fig. 51:   Comparison of FLUENT and Flow-3D pressure time history with experiment 3a
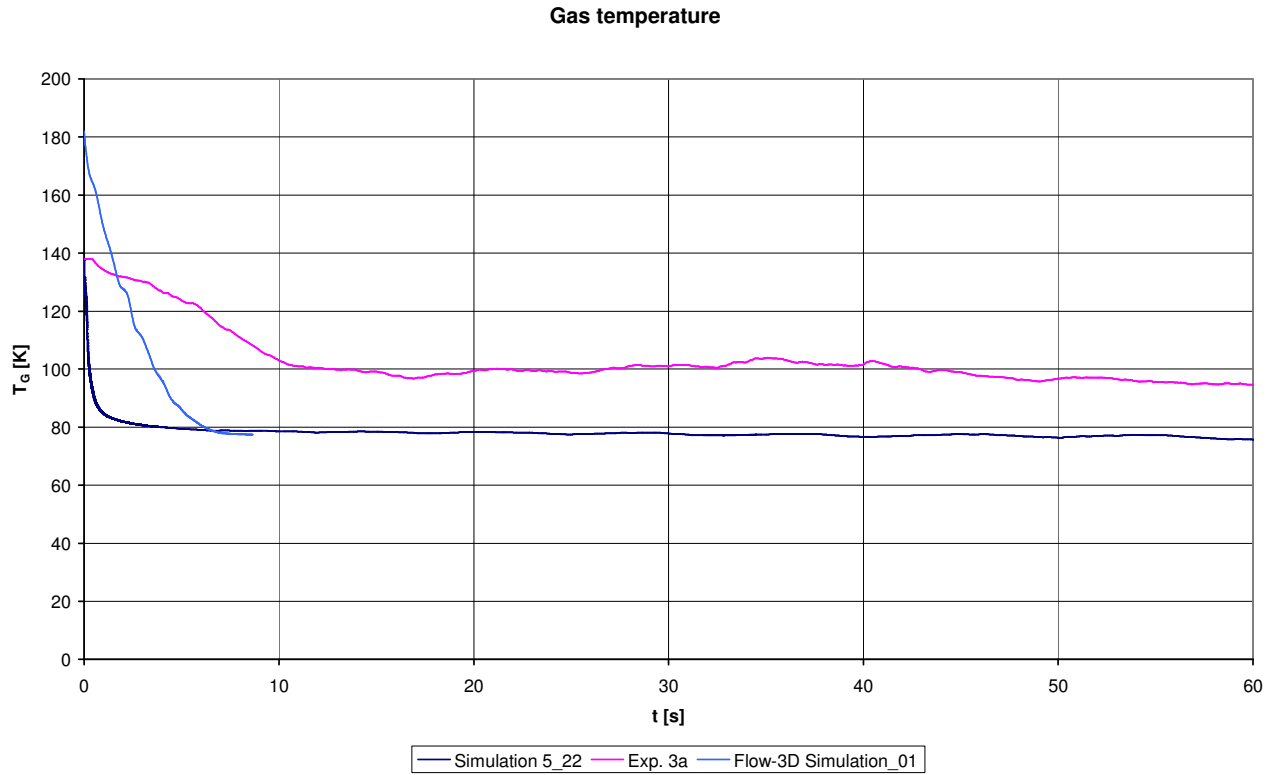
Gas temperature

Fig. 52:   Comparison of FLUENT and FLOW-3D gas temperature time history with experiment 3a

5.7 Second Benchmark Test Cases

5.7.1 Non-isothermal re-orientation

Goal of the non-isothermal re-orientation in frame of the second benchmark tests was to assess the re-orientation of the interface layer at reduced gravity. A Flow-3D model was generated. Test liquid was HFE 7000.

Input data for FLOW-3D analysis were:
- Mesh: 140 x 372 mesh
- Full energy equations solved in fluid (2nd order monotonicity preserving, implicit)
- Laminar viscous flow with no-slip condition
- Temperature dependent surface tension (implicit)
- Temperature dependent density
- Other conditions according to ZARM benchmark document

Test case 14 (200 W case) was considered for the assessment. FLOW-3D plots of the reorientation process are shown in Fig. 53.
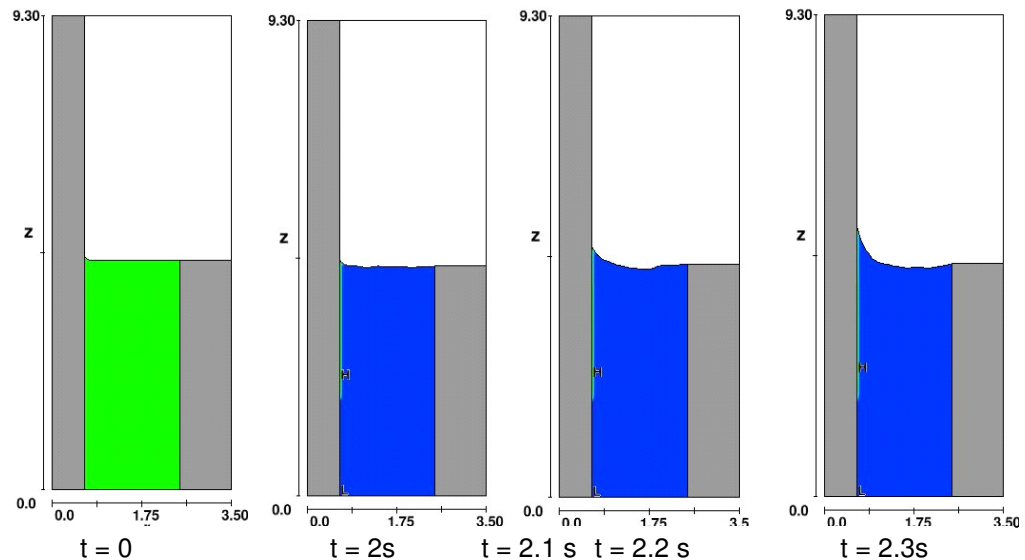
Fig. 53: Non-isothermal reorientation for test case 14 (200 W case) with 2 s waiting phase at 1g

For certain temperature regimes a liquid layer has formed in the experiment. In the present benchmark test case the evaluation of this layer has been omitted. In order to compare the numerical results with the experimental one an "apparent contact" angle was defined. A sketch of the situation at the heater wall when a liquid layer is present, including the location of the apparent contact angle, is shown in Fig. 54.
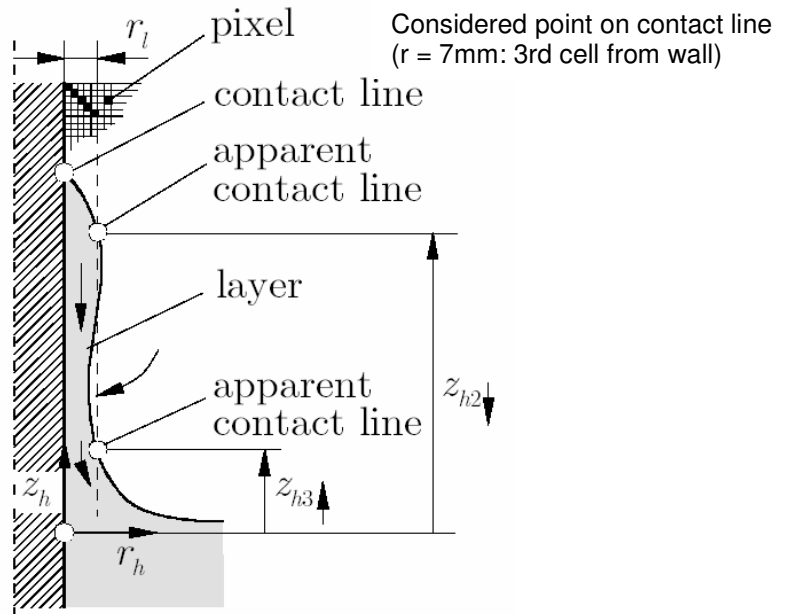
Fig. 54: Definition of contact zone elements

Fig. 55 shows the results of the FLOW-3D simulation with respect to the height of the apparent contact angle z_h (including smoothed results with FFT analysis).
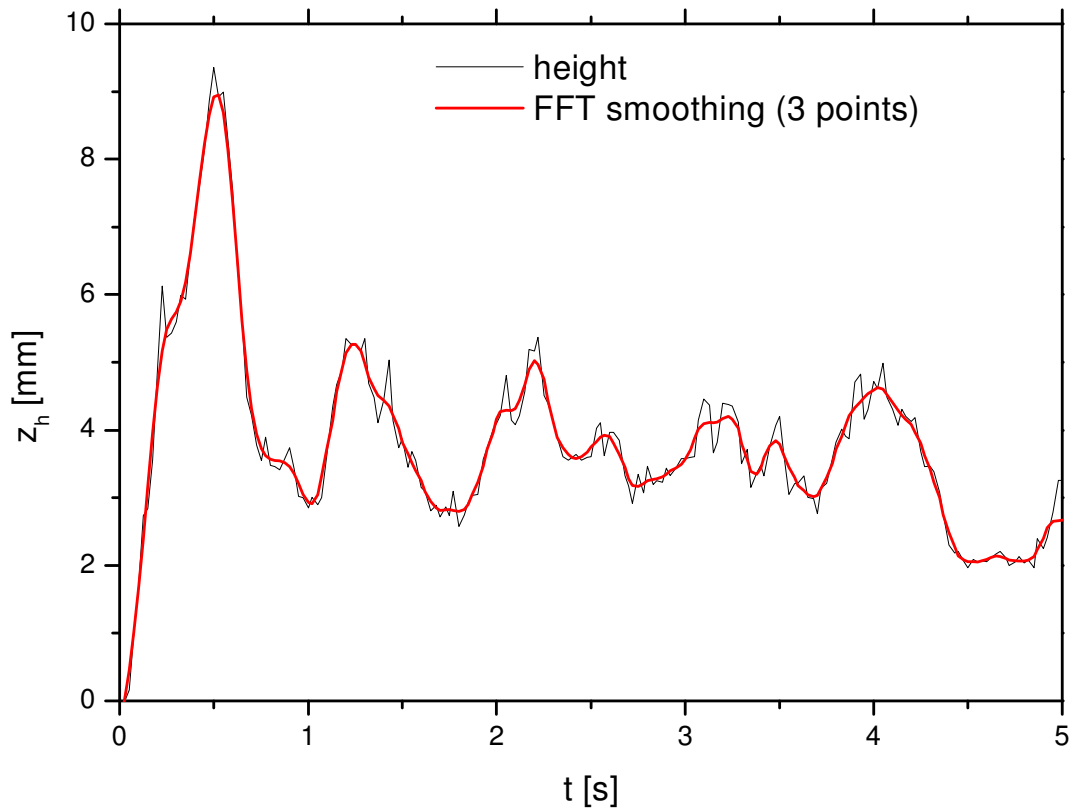

Fig. 55: Test number 14: Height of the apparent contact line as function of time (with FFT smoothing result)

The numerical analysis included the presence of a liquid layer, shown in Fig. 56.
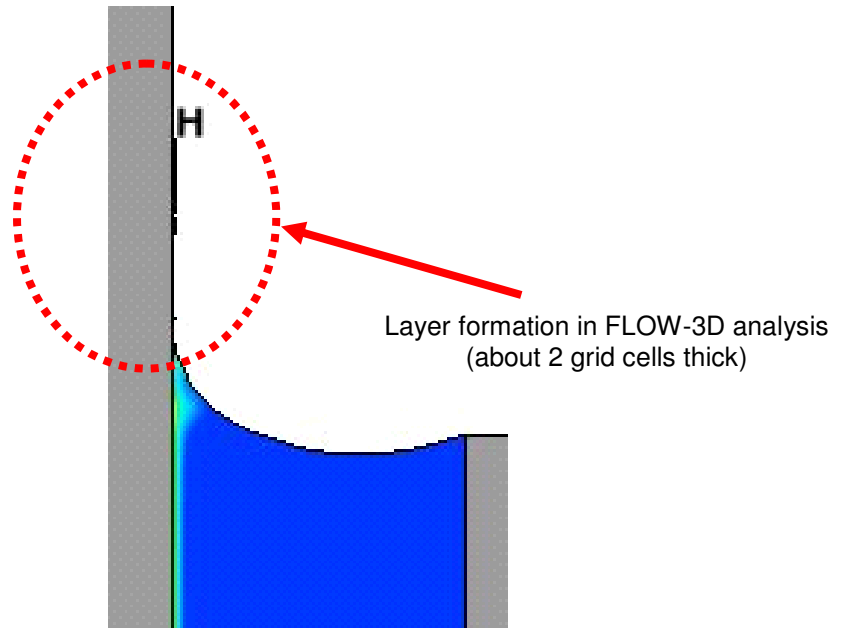
Fig. 56: Layer formation in Flow-3D analysis at test number 14

The layer was observed in the numerical model. In the experiment it was not clearly possible to assess the existence of such a layer formation. The assessment of the layer formation could be a useful work for further research.
Fig. 57 shows the derivative of the FFT smoothed data which is the velocity of the apparent contact line in z-direction.
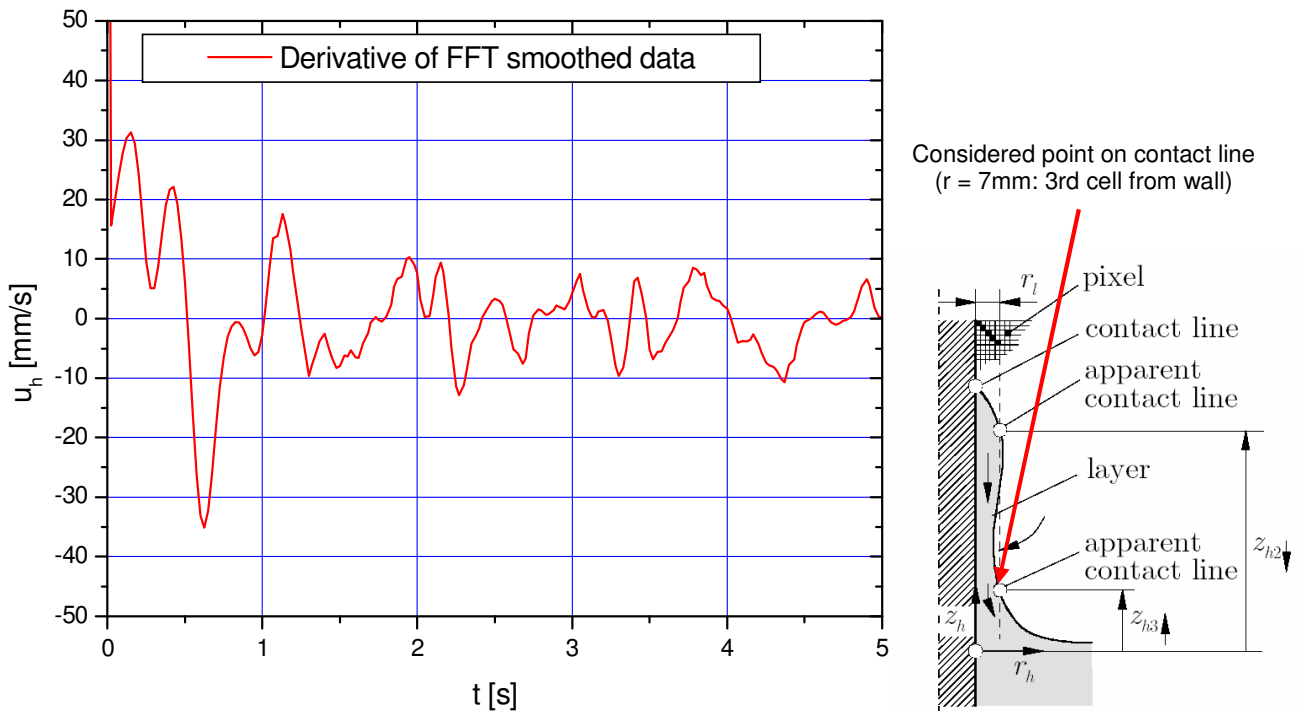

Fig. 57: Test number 14 derivative FFT smoothed data

The obtained apparent contact angle is shown in Fig. 58.

Model 1 of test number 14 (140x372 grid)
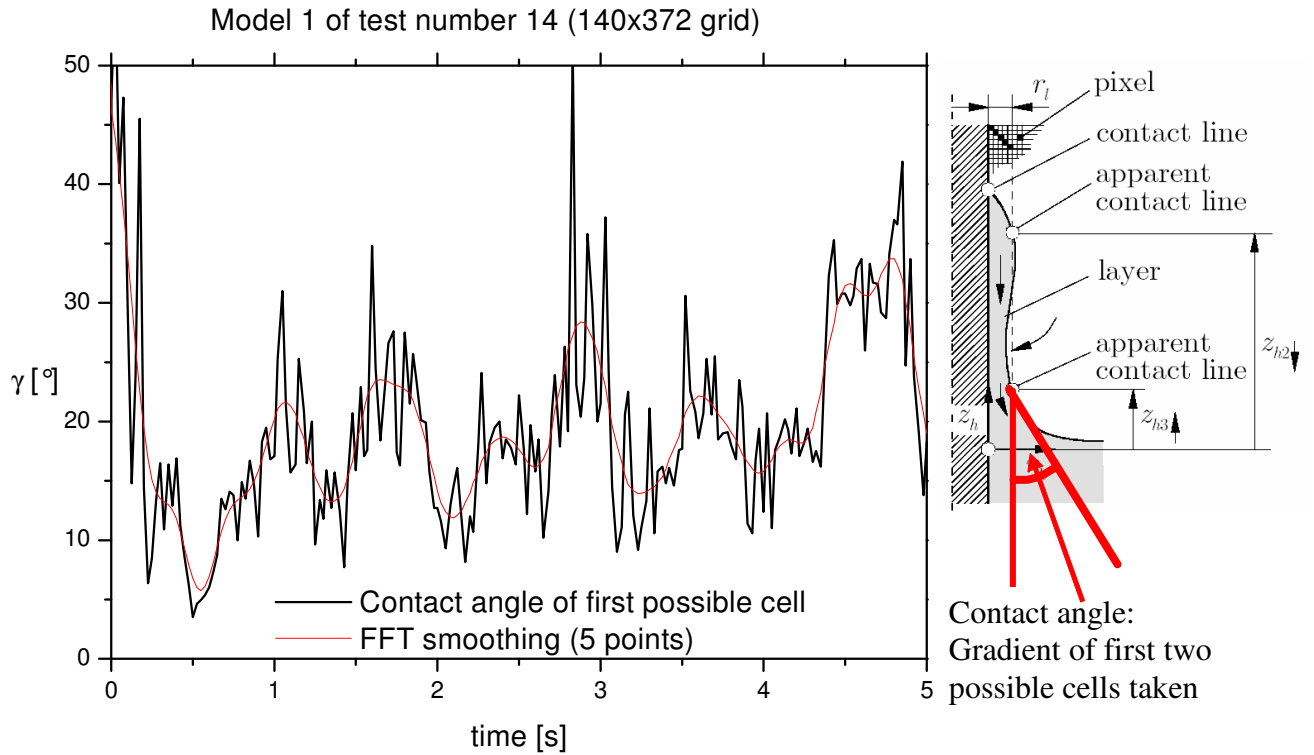
Fig. 58:   Test number 14 contact angle gradient estimation

Thermal Assessment

The FLOW-3D model included the analysis of the heat transfer within the heater (see Fig. 59).
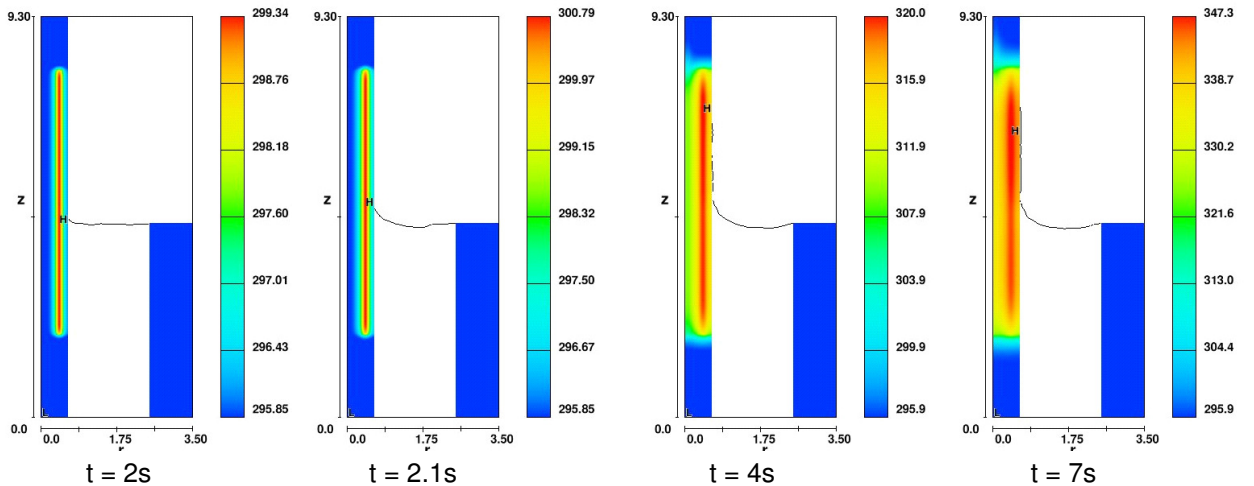

Fig. 59: Test number 14 wall temperature contours

Fig. 59 depicts the non-isothermal re-orientation during t=2s (drop from 1g to 0g) and t=7 s. The colour bar to the right of the diagram shows the temperature gradient. In the investigated test case it can be seen that the temperature in the wall increases as function of the time.

The temperatures have been monitored at different sensor points on the heater, plotted in Fig. 60.
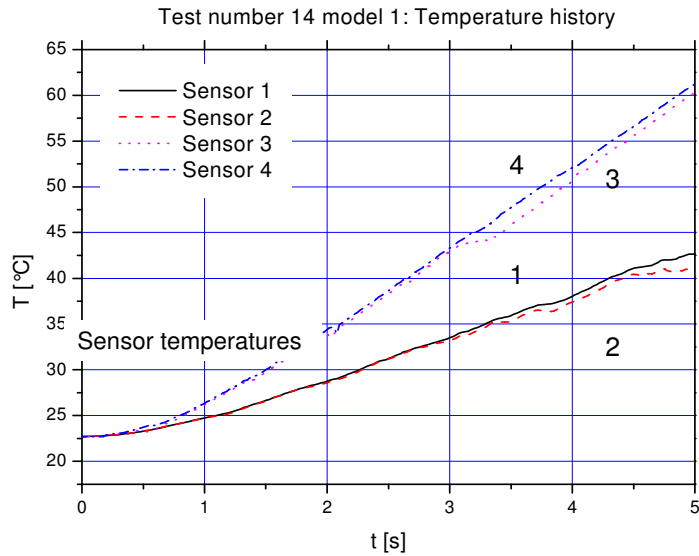
Fig. 60:   Test number 14 temperature sensor history

The estimated temperatures correlate well with the experimental results. Generally a strong temperature gradient exists near the heater surface. Thus a strong influence with respect to the applied mesh can be expected. Two different mesh resolutions were therefore calculated. The resulting contact angle apparently shifts when the grid resolution is increased (see Fig. 61).
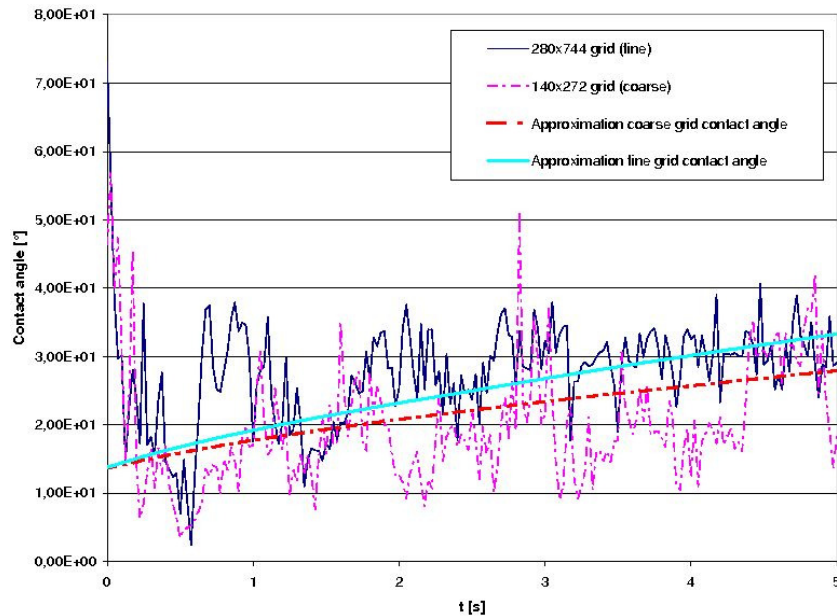

Fig. 61:   Approximation of the contact angle for different grid resolutions (140x272 and 280x744 grid)

Conclusion
The following conclusions may be drawn based on the non-isothermal reorientation benchmark (test number 14):
The agreement between numerical and experimental results is very promising. However, generally a very fine grid should be chosen in order to achieve a good approximation. The results converge towards the experimental solution when the grid is refined.

The influence of Marangoni convection is very much dependent on the resolution of the grid near the heated boundary. Thus investigations were carried out with two grids, one half the size of the other. Generally the

numerical grid would have to be very fine at the solid wall in order to give accurate results. For launcher applications this is generally not the case. It can be therefore expected that for upper stage configurations (stage diameter is 5.4 meters) the solution will not be as accurate as in the present benchmark test case. It is therefore proposed to adapt the boundary condition at the wall which takes into account the change concerning contact angle as a function of the local temperature. The following relation seems to be suitable based on the experimental results:

$$\gamma_{shift} = \alpha \left(\frac{We}{We_M} \right)^{\beta}$$

The two coefficients α and β have been obtained from the experimental results.

5.7.2 Geysering phenomena

The second test case consists of a geysering experiment performed under 1g conditions. At t=0 a membrane which kept the liquid at the top of the test chamber was destroyed. The liquid then reorients towards the bottom of the test tank. Different time steps of the FLOW-3D simulation are shown in Fig. 62. Test liquid is water.
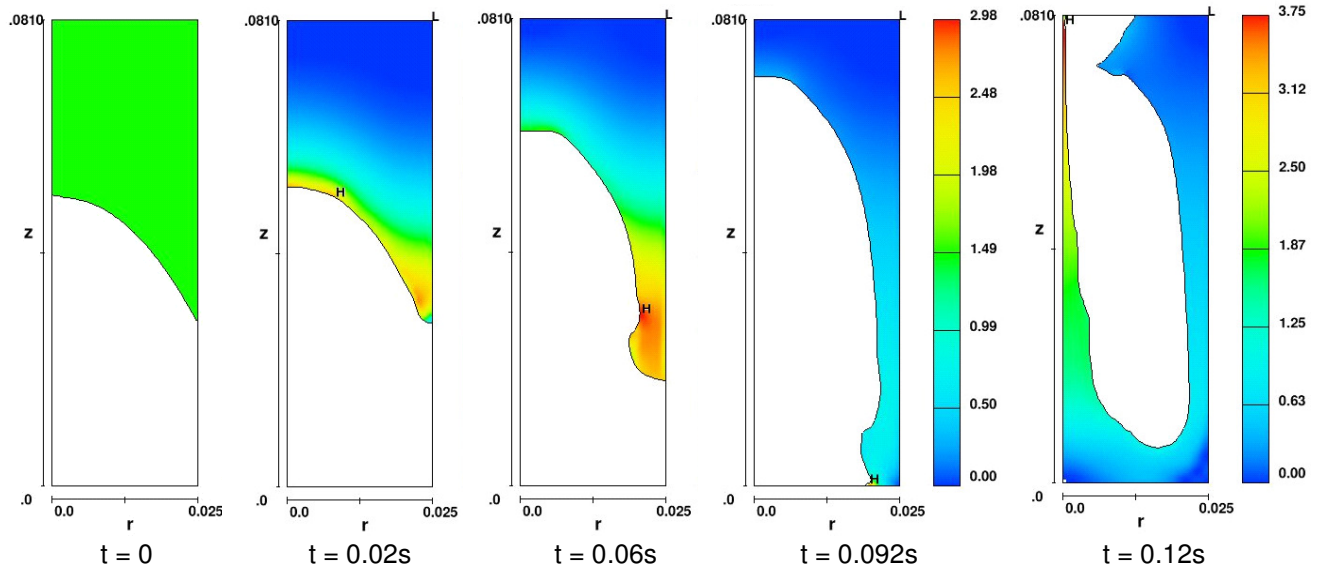

Fig. 62: FLOW-3D plots of the reorientation process

Fig. 63 shows the motion of the centre line and the contact line at the tank wall. Both theoretical as well as numerical and experimental results are plotted.
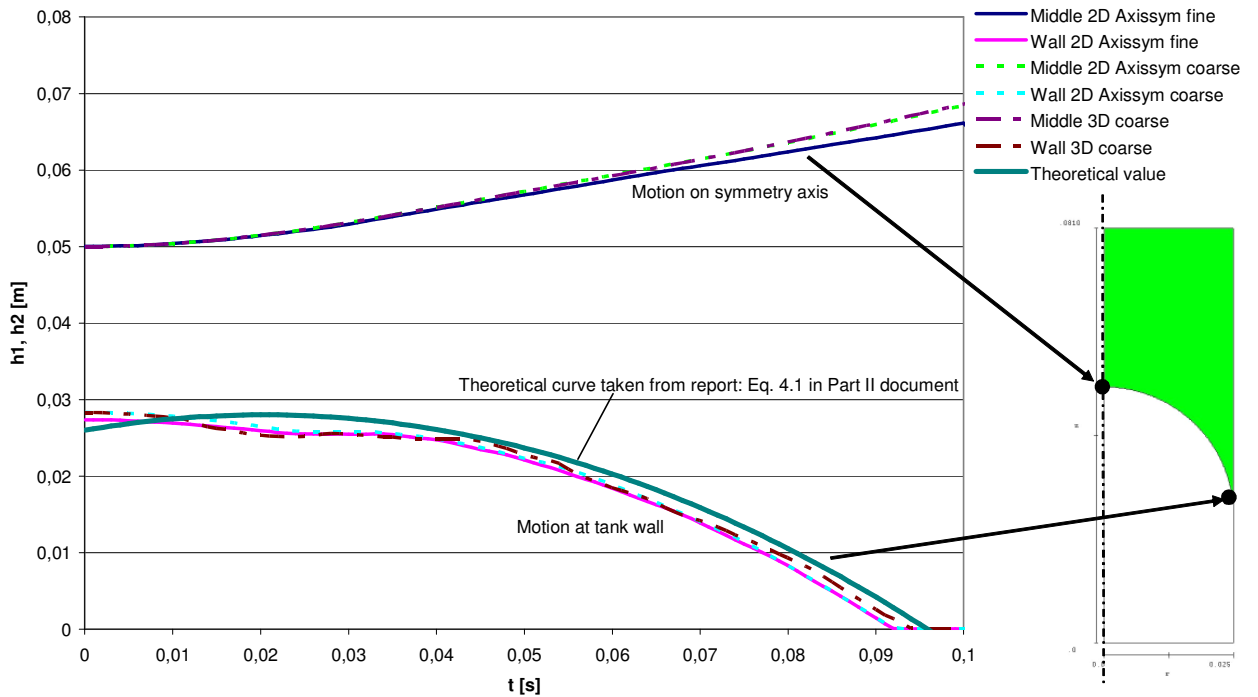
Test Case 1 Tap Water

Fig. 63:   History plots of centre line and contact line motion (theoretical, numerical and experimental results given)

It can be seen that the results have a good correlation. The assessment of the geyser itself was also part of the benchmark analyses.

Application of the geysering model

Geysering is a common phenomenon in upper stages. One example where geysering may occur is thus outlined in the following.

Stage spin has a major impact on the restart of the engine at the end of a coasting phase. Tank rotation will direct the liquid away from the tank outlet which is located at the tank bottom (see following picture at t=0 -- example of ESC-B LOX tank) [RD 8].

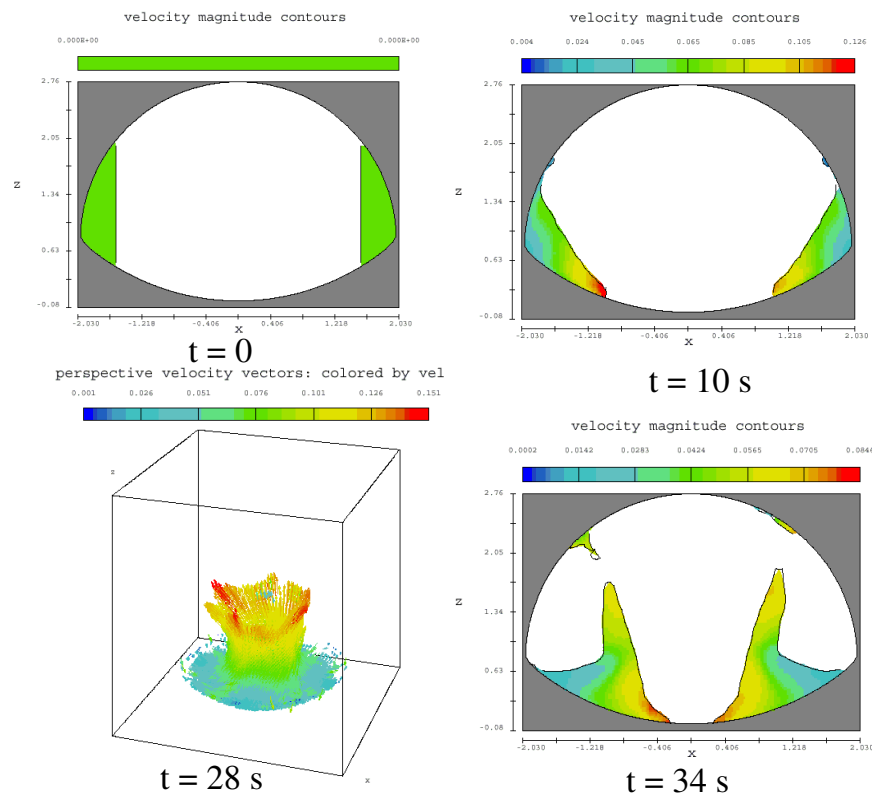a = 8 10^{-3} m/s², 1 °/s constant spin

Fig. 64: Re-orientation of the liquid in the ESC-B LOX tank in case of low acceleration with constant spin (1 °/s)

In case no internal devices such as baffles are present, large disturbances may occur (compare pictures above). Geysering in cryogenic tanks leads to a strong mixing of the ullage gas. This may result in destratification which leads to pressure variations in the tank. Possibly in some cases the variations are too quick in order to be balanced by the stage's pressure system. This point is therefore of great relevance for the layout of future upper stages. Numerical tools such as FLOW-3D which are able to describe the geysering process are in any case required for the analyses.

5.7.3 Isothermal Bubble Behaviour

This test case describes experimental investigations which were carried out with liquid nitrogen. Goal of the experiments was to investigate the behaviour of a single vapour bubble. To generate a bubble a PT100 heater was placed within a pressure vessel. The test setup is shown in the following picture.
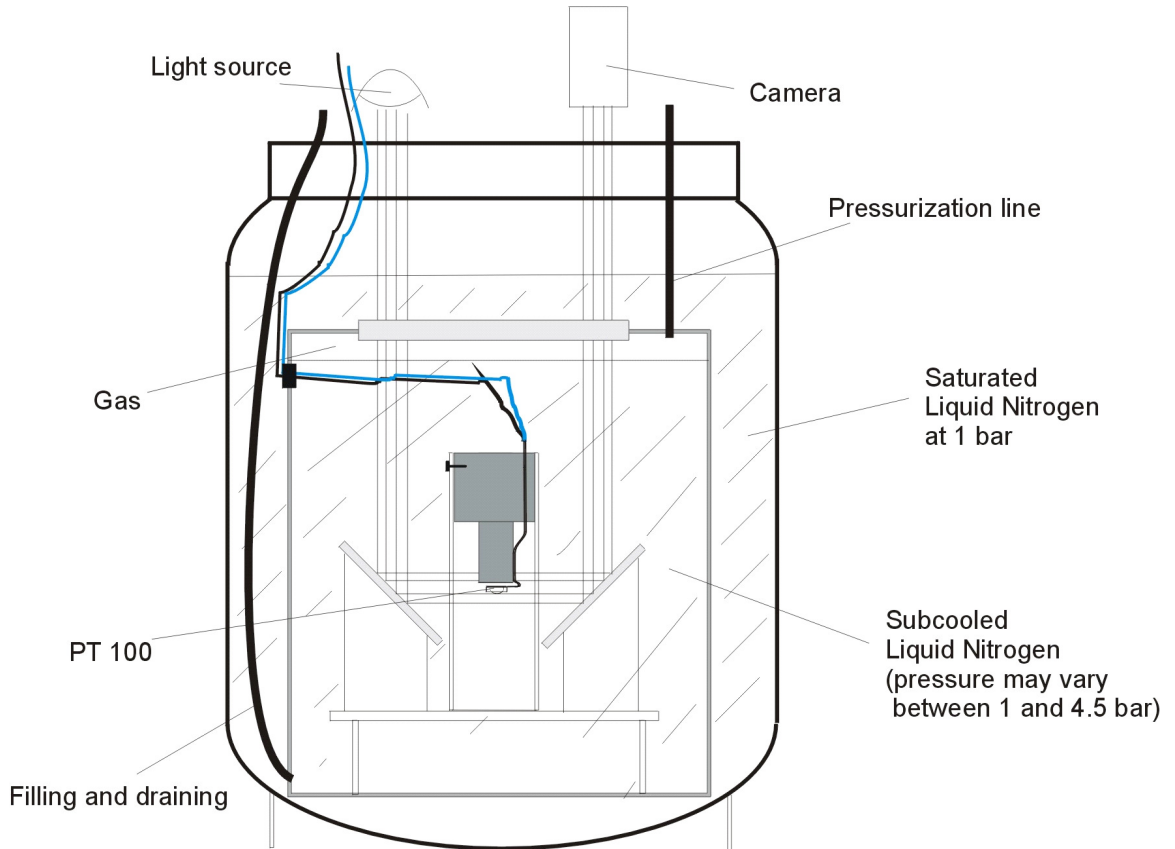

Fig. 65:   Test setup single bubble experiment

A cylindrical container is submerged in saturated liquid nitrogen keeping a constant temperature at the boundaries of the container (saturation temperature at 1bar). The inner container can be pressurized up to 4.5 bar. The higher the pressure, the more subcooled is the liquid in the inner container since the temperature stays nearly constant. A PT100 temperature sensor was used to introduce a heat flux into the test vessel at the beginning of the experiment. The PT100 at the same time measured the local temperature.

The test setup allowed holding a vapour bubble stable in place by implementing a bubble trap around the PT100. A glass window and two mirrors inside the pressure container allowed the bubble to be monitored from the top of the vessel (see optical path in above picture). A picture of the PT100 submerged in liquid nitrogen can be seen in the following picture.

Depending on the pressure and thus the subcooling of the liquid the required power was measured to form stable bubbles of comparable sizes. In the picture below, the liquid (at p = 3 bar) was heated with 0.55 W. A bubble formed below the PT100 heater. Flow marks due to convection are also visible at the side and top of the bubble trap.
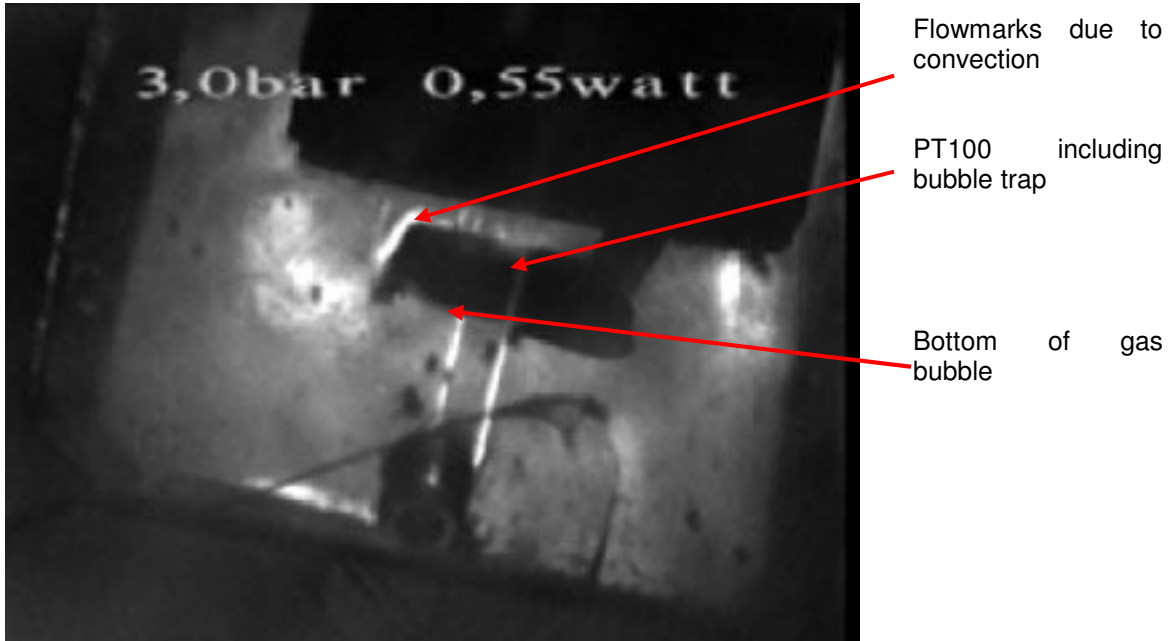
Fig. 66:   Picture of the PT100 and the bubble trap

A number of temperature sensors were placed around the PT100 in order to measure the temperature around the forming gas bubble (see following pictures).
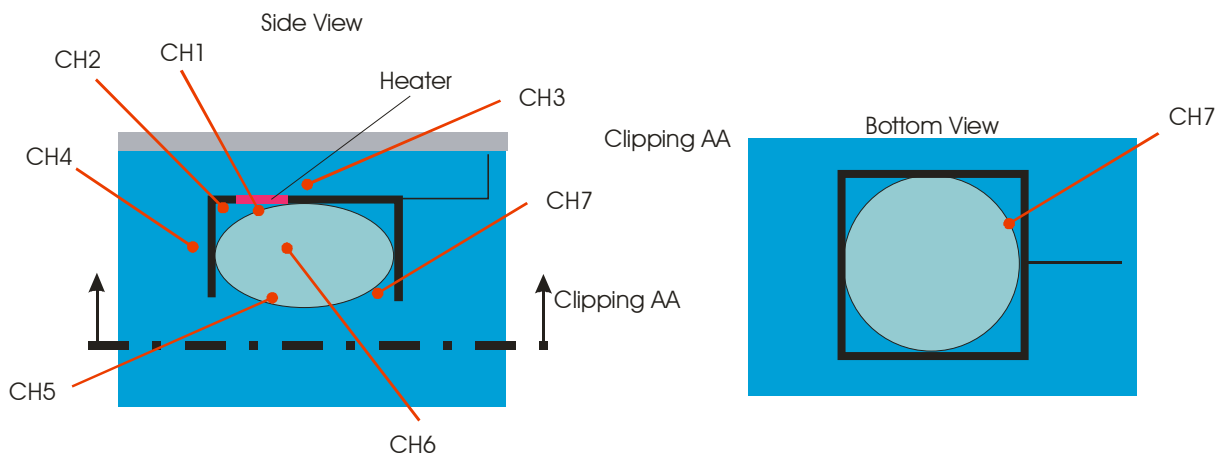

Fig. 67:   Temperature sensors around PT100 temperature sensor

The test setup showed that the bubble can be kept steady below the PT100 heater. The heat flux into the liquid is known including the temperatures at certain locations. Thus, the bubble behaviour can be estimated numerically using the obtained data. Preliminary analyses were started with the software FLOW-3D.

5.7.4 Investigation of Marangoni convection using available literature data

Experimental analyses by Betz and Straub in [RD 12] were used as a first step to investigate the capability of FLOW-3D to calculate the flow (driven by Marangoni convection) around a single gas bubble. A non-condensable gas bubble was submerged in a non-cryogenic liquid as shown in the following picture, left side.

The top and the bottom boundary of the liquid were kept at different temperatures. Thus, a temperature gradient forms which leads to Marangoni convection. Different liquids were analyzed. The same test case was calculated with the software FLOW-3D. The result of the FLOW-3D analysis is shown on the right side of the following picture.
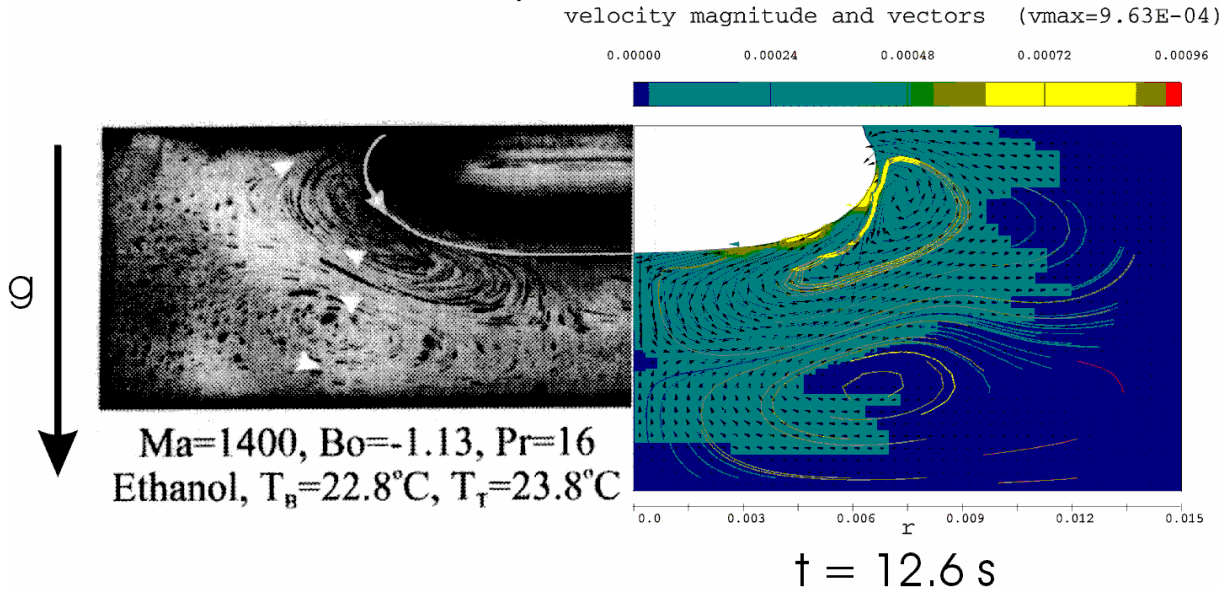
Fig. 68: Comparison of an experiment, described by Betz and Straub [1], and the corresponding FLOW-3D calculation

Similar numerical analyses were carried out by Betz and Straub. A comparison of the numerical results obtained by Betz and Straub and the corresponding FLOW-3D result is given in Fig. 69.
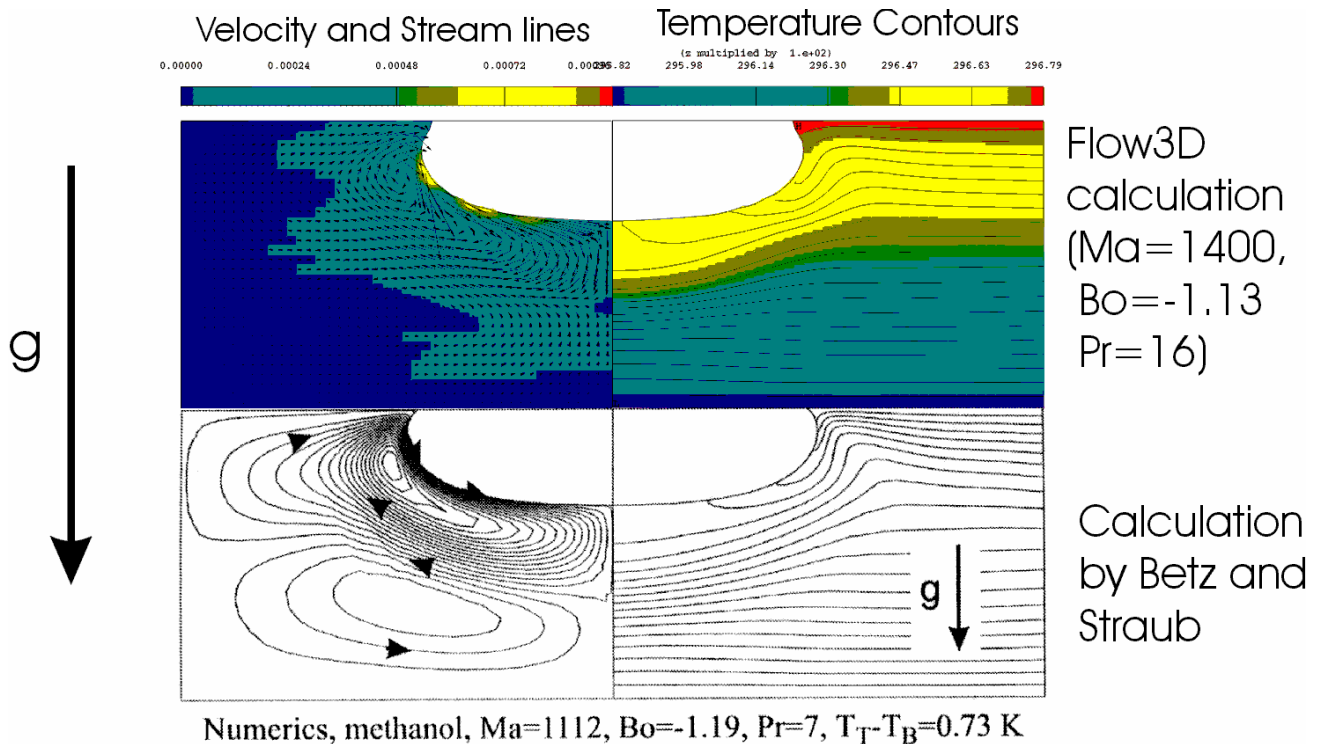

Fig. 69: Comparison of numerical analysis described by Betz and Straub and the corresponding FLOW-3D calculation

The FLOW-3D results fit very well to the experimental and the numerical results calculated with numerical analysis described by Betz and Straub. Thus the code is able to simulate Marangoni convection in the above case.

6. Conclusion

The present document summarizes the work which was carried out in the frame of the COMPERE project. Main focus is to assess and develop the capabilities of numerical software codes such as FLOW-3D which are required for future analyses. A number of benchmark experiments were therefore generated which allow a crosscheck with the computer codes. Based on the results of the different benchmark experiments the following points may be summarized.

➢ The FLOW-3D software performs well in cases of sloshing, geysering, 0g, stratification, Marangoni convection. A very good understanding was obtained which allows a much better judgement of numerical results. The performed benchmark experiments prove the code capabilities. This is essential for the layout of future upper stages.

➢ The performed tasks allowed detecting limitations with respect to the code capabilities. One example is the behaviour in case of sloshing damping. Sloshing damping is generally too high. This task has to be taken into account when evaluation e.g. the settling time when liquid reorientation occurs in a tank.

➢ Handling of two phases, liquid and gas, is still difficult. Especially the evaluation of surface tension effects seems to be problematic.

➢ Boiling phenomena still pose a difficult task for the available CFD tools. Different analyses have been initiated to assess the code's accuracy and to develop required physical models. The assessment of these phenomena should therefore be considered as a main task for future projects. Main relevance with respect to future upper stages are the planned ballistic flight phases where boiling and other phase change phenomena will occur.

➢ For launcher applications the different sizes, large tank and e.g. small bubbles, poses a problem if modelled with a CFD tool. Thus, based on the performed tests and numerical analyses alternative models were proposed. In case of boiling models a particle model was proposed which allows the simplified modelization of bubble motion in the stage tanks. The development of these tools and their optimization is a task to be carried out in the future.

7. Acknowledgement

The members of the COMPERE team at Astrium would like to thank the Deutsches Zentrum für Luft- und Raumfahrt (DLR) for their support.